

# Sea-level changes across the Paleocene–Eocene interval in the Spanish Pyrenees, and their possible relationship with North Atlantic magmatism

Victoriano Pujalte <sup>a,\*</sup>, Birger Schmitz <sup>b</sup>, Juan Ignacio Baceta <sup>a</sup>

<sup>a</sup> Department of Stratigraphy and Palaeontology, Faculty of Science and Technology, University of the Basque Country UPV/EHU, Ap. 644, 48080 Bilbao, Spain

<sup>b</sup> Division of Nuclear Physics, Department of Physics, University of Lund, P.O. Box 118, SE-221 00 Lund, Sweden



## ARTICLE INFO

### Article history:

Received 11 October 2012

Received in revised form 23 October 2013

Accepted 31 October 2013

Available online 9 November 2013

### Keywords:

Sea-level changes

Paleocene–Eocene interval

PETM

Pyrenees

N Atlantic magmatism

## ABSTRACT

The issue of whether major and rapid global sea-level changes existed on a preglacial Earth can be resolved by the detailed study of the Paleocene–Eocene (P–E) interval, where a large and rapid carbon isotope excursion linked to an important global warming event, the Paleocene Eocene Thermal Maximum, allows for high-resolution correlation between terrestrial, coastal and marine settings. Based primarily on outcrop and borehole information from the Tremp-Graus Basin in the southern Spanish Pyrenees, it is shown that a sea-level fall of at least 20 m occurred less than 75 kyr prior to the PETM. This forced a seaward displacement of the shoreline of ca. 20 km, a widespread incision of valleys in the alluvial plains and the subaerial exposure and excavation of the adjacent marine carbonate platform. The subsequent sea-level rise caused the infilling of the incised valleys, a process completed before the onset of the PETM, and continued rising during and after the event, leading to the aggradation of the alluvial plain and eventually to the transgression of the whole Tremp-Graus Basin. However, the sea level did not regain its pre-fall position until near the end of the PETM. Therefore, although rising, the sea level was comparatively low in the southern Pyrenean area during most of the PETM. The pre-PETM sea-level fall has been reported in other basins of the southern Pyrenees, in the North Sea area, the Austrian Alps and in Egypt, and the subsequent sea-level rise has been documented in widely separated sites around the Earth, an evidence of their global (eustatic) scope. The causal mechanism(s) of the pre-PETM sea-level fall is (are) unresolved, although glacioeustasy may have played a role. The subsequent sea-level rise was most likely caused by tectonomagmatic activity in the North Atlantic.

© 2013 Elsevier B.V. All rights reserved.

## 1. Introduction

The Paleocene Eocene Thermal Maximum (PETM) was the most prominent of several geologically brief episodes (< 200 kyr) of extremely high temperatures which interspersed the warm early Paleogene greenhouse climate. It is well documented that during the PETM, which occurred ca. 56 Ma ago, global temperatures rose by about 5–9 °C, causing a significant biotic impact (e.g., Thomas, 1998; Crouch et al., 2001; Gingerich, 2003). The fingerprint of the PETM is a 2–6‰ negative carbon isotopic excursion (CIE), identified in many ocean sediment cores and land-based sections (e.g., Zachos et al., 2003; Aubry et al., 2007). The CIE developed in less than 20 kyr (McInerney and Wing, 2011) requiring the rapid addition of massive quantities of isotopically light carbon to the atmosphere-ocean reservoir.

Yet, the trigger of the PETM remains controversial. Alternative hypotheses include, among others, destabilisation of oceanic methane hydrates (Dickens et al., 1995), thermogenic CO<sub>2</sub> and CH<sub>4</sub> production in the North Atlantic (Svensen et al., 2004), orbitally triggered carbon

release from the thawing of circum-Arctic and Antarctic terrestrial permafrost (DeConto et al., 2012) and the oxidation of organic matter after the desiccation of a large epicontinental seaway (Higgins and Schrag, 2006). The latter hypothesis required a “relative sea-level fall prior to the onset of the CIE”, a possibility that Higgins and Schrag (2006, p. 531) supported with literature data, including a study by Schmitz et al. (2001). Indeed, Schmitz et al. (2001), and later Schmitz and Pujalte (2003) inferred from their studies in the Pyrenees that the PETM might have occurred during an interval of low sea level. Some authors, however, have challenged a pre-PETM sea-level drop (e.g., Sluijs et al., 2008).

The purpose of this paper is to reassess sea-level changes across the Paleocene–Eocene (P–E) interval based primarily on evidence from the South Pyrenean Tremp-Graus Basin, but also with data from a selection of other basins. It is shown that in the Tremp-Graus Basin: 1) there is clear proof that a sea-level fall occurred shortly before the onset of the PETM; 2) the subsequent sea-level rise was initiated before the onset of the PETM and continued during and after the event; and 3) although rising, the sea level stayed relatively low during most of the PETM. The published results from other basins in the Pyrenees and elsewhere seem to confirm that the range of the reported sea-level changes was at least

\* Corresponding author. Tel.: +34 946012606; fax: +34 6013500.

E-mail address: victoriano.pujalte@ehu.es (V. Pujalte).

supra-regional if not global. Finally, a possible link between North Atlantic tectonomagmatic activity in the North Atlantic and the sea-level rise across the P-E interval is discussed.

## 2. Geological setting

The Pyrenean orogen resulted from the Late Cretaceous to Early Miocene collision between the Iberian and European plates (Roest and Srivastava, 1991). Its axial zone, formed mostly of Palaeozoic basement, is flanked to the north and south by thrust sheets of Mesozoic and Cenozoic sedimentary rocks with low-angle basal detachments (Muñoz, 1992). Three of these sheets are recognised in or near the study area, emplaced during the Santonian–late Maastrichtian, the Ypresian, and the Lutetian–early Miocene (Fig. 1; Fernández et al., 2012).

Tectonic quiescence prevailed during the latest Maastrichtian–earliest Ypresian, as demonstrated by slow and near homogeneous subsidence and the absence of angular unconformities or growth structures within the coeval succession. The studied succession was accumulated towards the end of this interval (Fig. 1), during which the main allocyclic controls of the sedimentation were climate and eustasy-dominated sea-level changes. The Ypresian Stage is, however, very long (8.2 Ma), and the local Ilerdian Stage is used here to allow for greater stratigraphic precision and because this stage name is used in

most of the literature on Pyrenean stratigraphy. It should be noted that the bases of the Ilerdian and Ypresian Stages are coeval (Pujalte et al., 2009a; Vandenberghe et al., 2012).

Throughout the P-E interval the Pyrenean domain was a deep-water embayment, opened westwards into the Bay of Biscay and flanked by shallow marine carbonate shelves. The shelves were surrounded by coastal alluvial plains that were particularly well-developed in the Tremp-Graus Basin due to an abundant clastic input from nearby mountains created during the Santonian–late Maastrichtian thrusting phase (Figs. 1, 2A).

## 3. Data set and methods

This paper partly draws on information from earlier studies, but mainly on new field and laboratory data. Earlier information includes several  $\delta^{13}\text{C}$  isotope profiles across the P-E interval from soil carbonate nodules, which for the first time allowed the delineation of the PETM in continental sections of Spain (Schmitz and Pujalte, 2003, 2007; Supplementary Fig. 1). Isotope profiles based on dispersed organic matter ( $\delta^{13}\text{C}_{\text{TOC}}$ ) of Domingo et al. (2009) have also been taken into account, as well as palaeontological information from marine Thanetian and Ilerdian deposits of Robador et al. (1990), Scheibner et al. (2007), Robador (2008) and Baceta et al. (2011).

Key new data include high-resolution maps across the P-E interval of three sectors of the Tremp-Graus Basin (Fig. 2B). The Esplugafreda sector is situated in the northern margin of the basin and was the last to be reached by the Ilerdian Sea. The Claret sector corresponds to the basin axis, the part of the basin showing the highest subsidence rate. The Esplugafreda and Claret sectors were situated in a coastal alluvial plain during Paleocene times, and were flooded by the sea after the PETM. In contrast, the Campo sector was in a marine setting during most of the Thanetian and Ilerdian times. The map of the Esplugafreda sector was included in a field guide of restricted circulation (Fig. 3.2 in Baceta et al., 2006). The maps of the other two sectors are published in this paper for the first time. New interpretations of borehole data across the P-E interval are also provided.

Also new are: 1) Field and  $\delta^{13}\text{C}_{\text{TOC}}$  isotope data from a new section, the Ferrera ridge (longitude:  $0^{\circ} 19' 59''$  latitude  $42^{\circ} 25' 28''$ ); 2) thin-section and polished-slab data from the Ferrera and Campo sections; and 3) micropalaeontological data from non-marine deposits across the P-E interval. Carbon isotopic analyses were performed with an Isoprime mass spectrometer with a dual inlet system, following standard procedures, at the Department of Geography and Geology at the University of Copenhagen. The results are listed in Table 1.

The micropalaeontological data were obtained by examining under a binocular microscope wet sieving residues of mudstone samples of several sections. In about half of the samples a scant assemblage (10–20 specimens) was found. Specimens with abraded and reddened tests, obviously resedimented, were ignored, but those with better-preserved tests and of colours similar to their host rocks were considered autochthonous or para-autochthonous. They are listed in Table 2, their environmental significance being discussed in the appropriate sections below.

## 4. Stratigraphy

Danian–lower Ilerdian successions of the Tremp-Graus Basin comprise two major facies, shallow marine and continental, which interfinger laterally and alternate vertically (Figs. 2B, C, 3). Shallow marine deposits mainly consist of carbonates that are rich in larger foraminifera (nummulitids, alveolinids and soritids), calcareous algae, molluscs and corals. Continental deposits, traditionally referred to in geological literature as “Garumian” or “Garumian facies”, are now included in the formally defined Tremp Group (Cuevas, 1992; Pujalte and Schmitz, 2005). This Group comprises several formations, of which only the upper two are relevant to this study (Fig. 2C). The

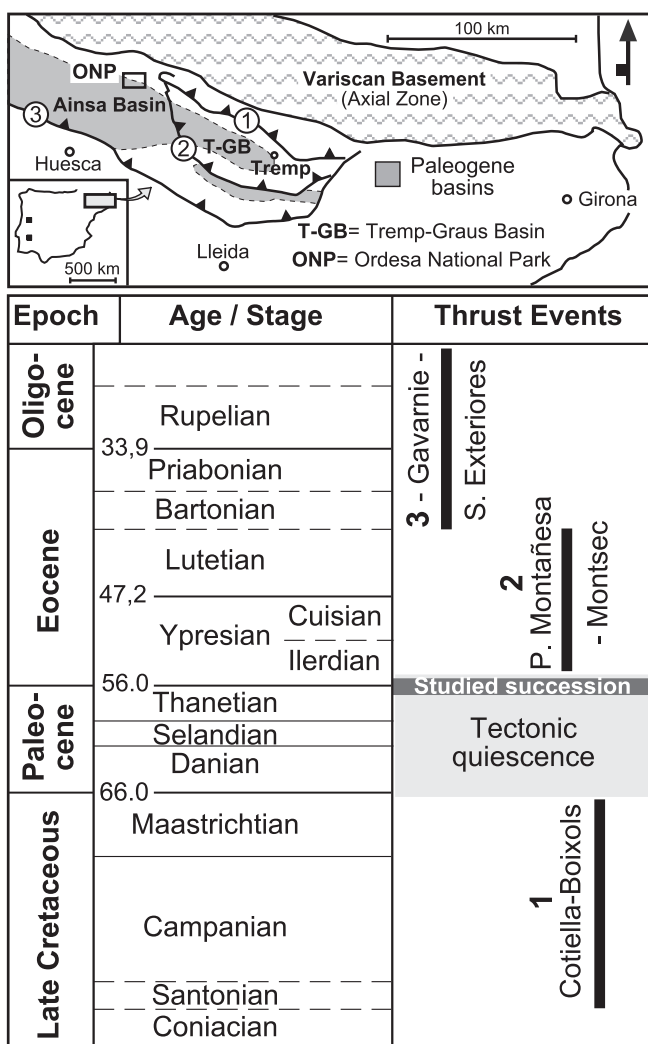


**Fig. 1.** Simplified geological map of the southern Pyrenees showing the position of the Tremp-Graus and Ainsa basins, and chronostratigraphic chart with indication of thrusting (i.e., tectonically active) and quiescent intervals (modified from Fernández et al., 2012).

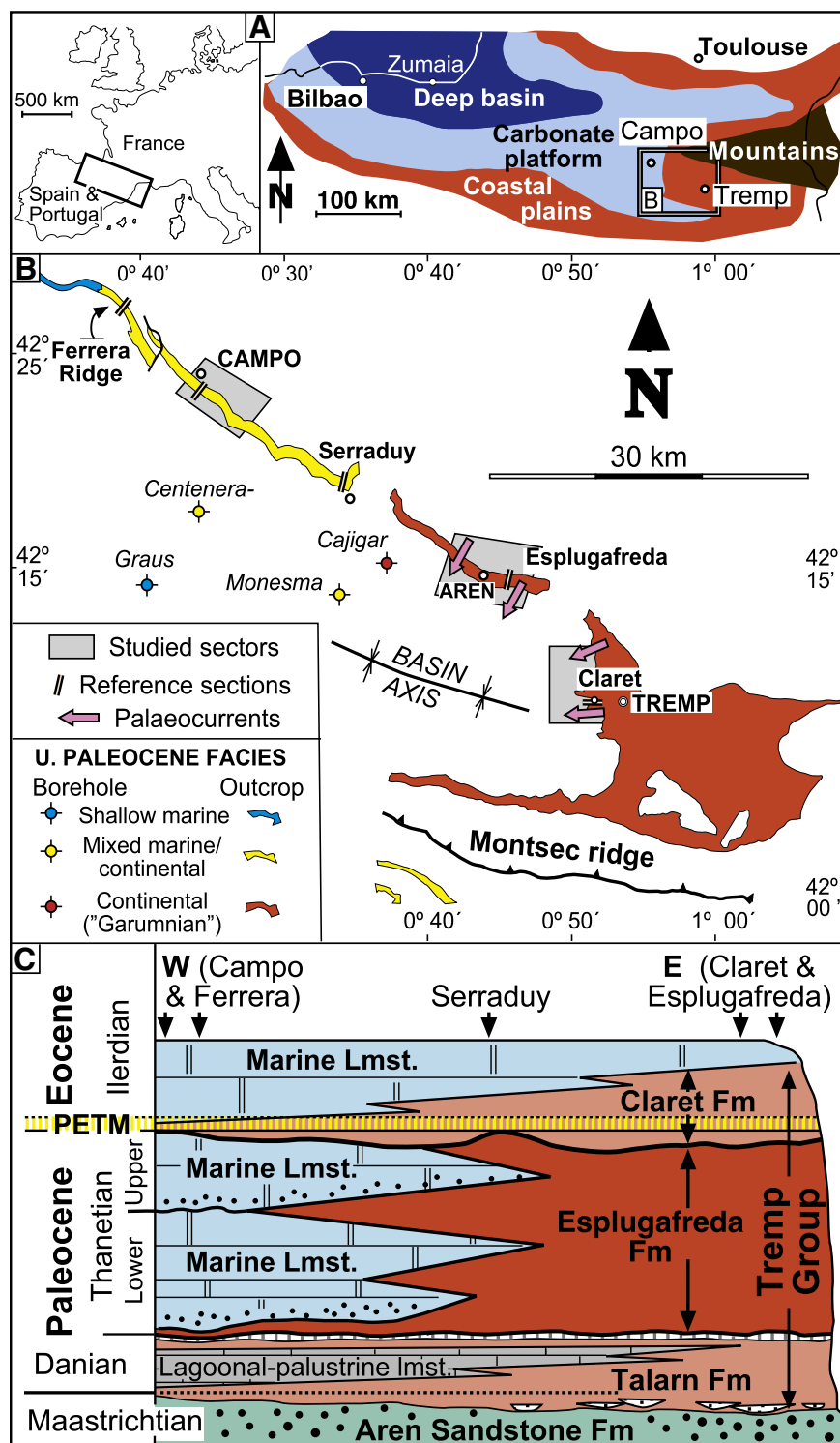


**Fig. 2.** (A) Location and early Paleogene palaeogeography of the Pyrenean area (B) Danian–Lower Ilerdian outcrops and facies of the Tremp–Graus Basin, with indication of the main study sectors (Esplugafreda, Claret and Campo), reference sections and boreholes. Palaeocurrents obtained mainly from imbricated clasts of conglomerate. (C) Simplified Danian–Lower Ilerdian stratigraphy of the Tremp–Graus Basin (after Cuevas, 1992, and Pujalte and Schmitz, 2005).

Esplugafreda Formation (Thanetian, 165–350 m thick) is mostly made up of overbank red silty mudstones with intercalated channelised calcarenites and calcareous conglomerates. In the Esplugafreda sector the red mudstones include numerous calcic soil horizons (K horizons of Gile et al., 1965) typified by abundant calcareous nodules 2–5 cm in diameter, and occasional horizons with gypsum veins and crystals. In the Claret sector, K horizons are somewhat less prominent but gypsum

is widespread, at some levels occurring as laterally persistent packages several metres thick. Both this gypsum and the ubiquitous K horizons provide evidence of an arid to semiarid climate.

The interfingering between the continental Esplugafreda Formation and the coeval marine carbonates is best observed in the Serraduy section (Fig. 2B, C). At Serraduy, the Danian is represented by a conspicuous 3.5 m thick unit of palustrine limestones overlain by a widespread soil

**Table 1**

$\delta^{13}\text{C}_{\text{toc}}$  values (‰ VPDB) and organic carbon content (wt%) of Claret Fm samples from the Ferrera section.

Sample	Lithology	$\delta^{13}\text{C}_{\text{toc}}$	wt%	Sample	Lithology	$\delta^{13}\text{C}_{\text{toc}}$	wt%
FE 6	Calcarenite	−27.3	0.10	FE 9	Clay	−26.36	0.41
FE 7	Calcarenite	−27.4	0.08	FE 10	Limestone	−27.99	6.92
FE 7r	Calcarenite	−27.3	0.10	FE 11	Limestone	−28.02	10.49
FE 8	Marl	−27.57	2.32	FE 12	Limestone	−29.31	14.50
FE 8r	Marl	−27.58	2.51	FE 13	Limestone	−27.81	23.36

Location of samples in Fig. 5. Samples with r indicate replicate analysis.

catena of stacked calcretes (Eichenseer, 1988; Robador et al., 1990; Fig. 3, Supplementary Fig. 2B). The bulk of the section above the soil catena consists of red mudstones with well-developed K soil horizons, the most typical facies of the Esplugafreda Formation. The red mudstones, however, contain two laterally extensive intercalations of mixed clastic/carbonate deposits, each 6–10 m thick, with larger foraminifera (Fig. 3, Supplementary Fig. 2A). The lower intercalation includes *Alveolina (Glomalveolina) primaeva*, *Idalina* sp., *Cribrobulimina* sp., and *Miscelanea yvetae*, while the upper one comprises *Alveolina (Glomalveolina) levigata*, *Alveolina aff. avellana*, *Alveolina aff. aramaea*, *Opertorbitalites gracilis* and *Orbitolites* sp. (Robador et al., 1990). These marine intercalations can thus be respectively assigned to the lower and upper Thanetian, both recording the easternmost location of the Paleocene shoreline in the northern margin of the basin.

The Claret Formation (10–70 m) is bounded below by a prominent erosional surface, and it is conformably overlain by marine Ilerdian limestones that are progressively younger to the east (Fig. 2C). Despite its comparatively modest thickness, the lithostratigraphy of the Claret Formation is quite varied, with one formal member (Claret Conglomerate Member, Pujalte and Schmitz, 2005), plus eight informal members having been recognised (Fig. 4), all of which have been age dated with isotopic data.

In the eastern part of the basin the Claret Formation is composed of five members, coded 1 to 5. Formal Member 2 (the Claret Conglomerate) and informal member 3 ("yellowish soils") were respectively accumulated during the onset and the core of the PETM, while member 4 was accumulated during the PETM recovery interval (Domingo et al., 2009; Fig. 4, Supplementary Fig. 1). Informal members 1 and 5 were respectively deposited before and after the PETM (Schmitz and Pujalte, 2003, 2007; Fig. 4, Supplementary Fig. 1).

Members 1, 2 and 3 can still be recognised in the Campo section, but with significant facies and thickness differences (Fig. 4). Further west, in the Ferrera ridge section, the Claret Formation is represented by four different informal members, coded I to IV (Figs. 4, 5). Total organic carbon isotopes from these four members are consistently quite light, ranging between −26.36‰ and −29.31‰ and averaging −27.66 (Table 1). These values are similar to those found by Domingo et al. (2009) within the Claret Conglomerate and the yellowish soils, implying that members I–IV at Ferrera belong to the PETM (Fig. 4).

This paper is focused on the palaeogeographical and sedimentological meaning of the basal unconformity and member 1 of the Claret Formation. Members of the Claret Formation accumulated during the PETM are also discussed, but more briefly.

## 5. Basal unconformity and member 1 of the Claret Formation: description

### 5.1. Esplugafreda sector

Panoramic outcrops in the Esplugafreda sector allow a direct observation in the field of the depositional architecture of the P–E interval. Three pre-PETM erosional depressions are recognised, named east, central and west in Fig. 6, which are up to 20 m deep and bounded by sharp, concave-up erosional surfaces cut into the predominantly bright red mudstones of the Esplugafreda Formation (Supplementary Fig. 3). The west and central depressions are ca. 1500 and ca. 1050 m wide, while the one in the east, composed of several amalgamated sub-depressions, is ca. 2000 m wide (Fig. 6). The depressions are infilled by fining-up successions of calcareous conglomerates and/or cross-bedded calcarenites grading-up into pale red mudstones with occasional intercalations of channelised calcarenites (Supplementary Fig. 3D), the infilling deposits onlapping the depression margins (Supplementary Fig. 3B). Imbricated clasts within the conglomerates and cross-stratification in the calcarenites indicate that currents flowed towards the SSW. The pale red mudstones contain sparse small-sized carbonate nodules indicative of weakly developed K soil horizons (cf., Wright and Marriot, 1996). These nodules yielded, in all cases, pre-PETM carbon isotope values (Schmitz and Pujalte, 2003, 2007; Supplementary Fig. 1).

The red colour of these member 1 deposits, together with the occurrence of carbonate soil nodules in the mudstones, are indicative of alluvial processes. The fining-upward character of the succession is thought to record diminishing flows through the depressions as they became progressively filled. The Claret Conglomerate rests on a relatively flat surface, either overlying deposits of member 1 or directly those of the Esplugafreda Formation (Fig. 6; Supplementary Fig. 1). It is clear, therefore, that the excavation and infilling of the depressions was completed before the onset of the PETM.

### 5.2. Claret sector

Two erosional depressions have been recognised in the N–S oriented outcrops of the Claret sector, one around the hamlet of Claret, the other about 4 km to the north. The geometry of the former (Claret depression) has been fully reconstructed through careful mapping and the correlation of 8 sections (Fig. 7, Supplementary Fig. 4). This depression was ca. 1500 m wide and had an asymmetrical cross-section, being ca. 30 m deep in Section 4, its depth decreasing steeply to the north and more gently to the south. (Fig. 7B). Three main facies have been recognised, named A, B and C in Fig. 7B. Facies A forms the bulk of the infilling succession, while facies B and C only occur in the upper parts of Sections 4, 5 and 6.

Facies A is composed of three intermingled subfacies, coded A<sub>1</sub>, A<sub>2</sub> and A<sub>3</sub> (Fig. 7B). Subfacies A<sub>1</sub> is represented by cross-cutting channel-like bodies, each 1–2 m thick, made up of conglomerates grading upwards into cross-stratified calcarenites (Supplementary Fig. 5A, B). Clast imbrications within the conglomerates record westward flowing currents (Supplementary Fig. 5C). Subfacies A<sub>2</sub> is composed of calcarenites alternating with, and passing laterally into, grey-greenish mudstones (Supplementary Fig. 6A). Some calcarenite beds have

**Table 2**

Summary of autochthonous microfossils found in washed residues of mudstones of the Claret Formation.

Sample	Section/stratigraphic level	Microfossils (c = common; r = rare)	Salinity
CL-N1	Claret Section 4, member 1, subfacies A2	Charophyte oogonia (c)	Fresh
CL-Car 2	Claret Section 6 member 1, facies B	small benthic foraminifera (c), gastropods (r), charophyte oogonia (r)	Brackish (with fresh-water input)
CP-5	Campo section member 1	charophyte oogonia (c), ostracodes (r)	Fresh
CP-6	Campo section member 1	Gastropods (c), small benthic foraminifera (c) ostracodes (r), charophyte oogonia (r)	Brackish (with fresh-water input)
SF-8	Ferrera ridge section member II	Ostracods (c), small benthic forams (c), charophyte oogonia (r), gastropods (r)	Marine
SF-9	Ferrera ridge section member III	Charophyte stem (c), charophyte oogonia (r), gastropods (r)	Fresh

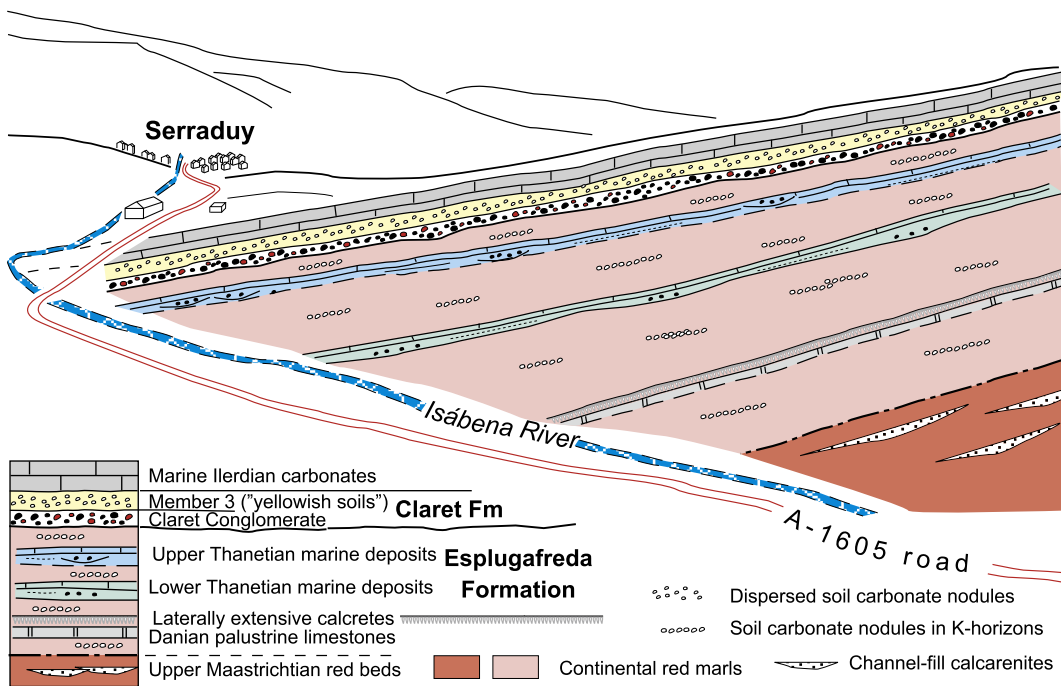


**Fig. 3.** Field sketch of the Serraduy section in the right (west) bank of the Isábena River, looking south (location in Fig. 2B). Thickness of the shown succession is ca. 150 m. Modified from Robador et al. (1990).

sharp erosive bases with flute and tool marks, parallel lamination in their lower parts and current-ripple lamination in their upper parts (Supplementary Fig. 6B, C). Others are entirely formed by unidirectional climbing ripples indicative of rapid sedimentation rates (Supplementary Fig. 6D). Palaeocurrents from these calcarenites usually diverge at nearly 90° from those of subfacies A<sub>1</sub>. The mudstones clearly represent a low-energy setting, the intercalated calcarenites recording episodic influxes of sediment-laden flows. Subfacies A<sub>3</sub>, which only occurs next to the northern margin of the erosional depression (Fig. 7B), consists almost exclusively of grey-greenish mudstones, with just occasional and thin intercalations of calcarenite beds. No evidence of soil development, such as carbonate nodules or rhizoliths, was observed in facies A. Small coal fragments were found within one bed of subfacies A<sub>1</sub>, and coalified plant remains are common within the calcarenite beds of subfacies A<sub>2</sub>. Washed residues from the mudstones of subfacies A<sub>2</sub> and A<sub>3</sub> were either barren or provided a few, poorly-preserved charophyte oogonia, indicative of fresh-water conditions (Table 2, sample CL-N1). Consequently facies A is collectively interpreted as fluvial, with subfacies A<sub>1</sub> representing channel-axis accumulations, subfacies A<sub>2</sub> levee/crevasse splay deposits resulting from discrete flood events, and subfacies A<sub>3</sub> floodplain deposits, their modest areal development being attributable to the confinement imposed by the depression margins. The predominance of grey colours in facies A, and the preservation of coalified remains, is indicative of poorly-oxygenated conditions.

Facies B is lithologically similar to subfacies A<sub>2</sub>, being also composed of an alternation of grey-greenish mudstones and calcarenites. However, a number of calcarenite beds from facies B are bioturbated by *Ophiomorpha* (Supplementary Fig. 6E), an ichnogenus indicative of marine influence. A few specimens of small calcareous benthic foraminifera found in the washed residue of sample CL-Car 2 (Table 2) are further proof of such influence, although the occurrence of charophyte oogonia in the same sample suggests occasional fresh-water inputs. Facies C is almost exclusively composed of red mudstones with scattered soil carbonate nodules (Supplementary Fig. 6F), features indicative of a well-oxygenated alluvial flood plain, its location attesting to the final infilling of the Claret erosional depression (Fig. 7B). The carbonate

nodules yielded pre-PETM isotopic values, a proof that such infilling was also completed before the onset of the event (Schmitz and Pujalte, 2007; Supplementary Fig. 1).

The erosional depression to the north of Claret is only partly exposed in an isolated outcrop (Supplementary Fig. 4D), and its dimensions could not be established. Its occurrence, however, demonstrates that more than one depression was excavated in the Claret sector. The depression fill is formed by a fining-up succession similar to those in the Esplugafreda sector.

### 5.3. Campo sector

The Campo section, the most representative of the Campo sector, provides many clues about the timing and magnitude of sea-level changes across the P-E interval, their appreciation requiring a brief description of the upper Thanetian succession. This succession is comprised of three mappable lithological units, coded L (lower), M (middle) and U (upper) in Fig. 8. These units are differentiated from each other by a contrasting lithology and in colour air photographs by a distinct shade, units L and U having a light brownish hue, the intervening unit M being light grey.

Unit L (14.5 m) rests abruptly on lower Thanetian dolomitic marls and limestones and it is composed of current-laminated quartz-rich packstones and grainstones with fragments of echinoderms, coralline algae and shallow benthic forams. Unit M (24 m) mostly consists of thickly-bedded bioclastic sandy packstones and grainstones rich in coralline algal fragments and/or shallow benthic foraminifera. The facies and fossils of both units, and the occurrence of a 7 m thick cross-stratified package within unit M (Fig. 8A), are indicative of a shallow marine high-energy environment. Units L and M are separated from each other by a ca. 6 m thick interval of marls and marly limestones, usually covered by vegetation (Fig. 8A), which contains an open marine fossil assemblage of ostracods and autochthonous calcareous nannofossils, including abundant specimens of *Discoaster multiradiatus*. This nannofossil allows assigning to geomagnetic chron C25n a short interval with normal polarities found within unit L (Pujalte et al., 2003; Fig. 8A).

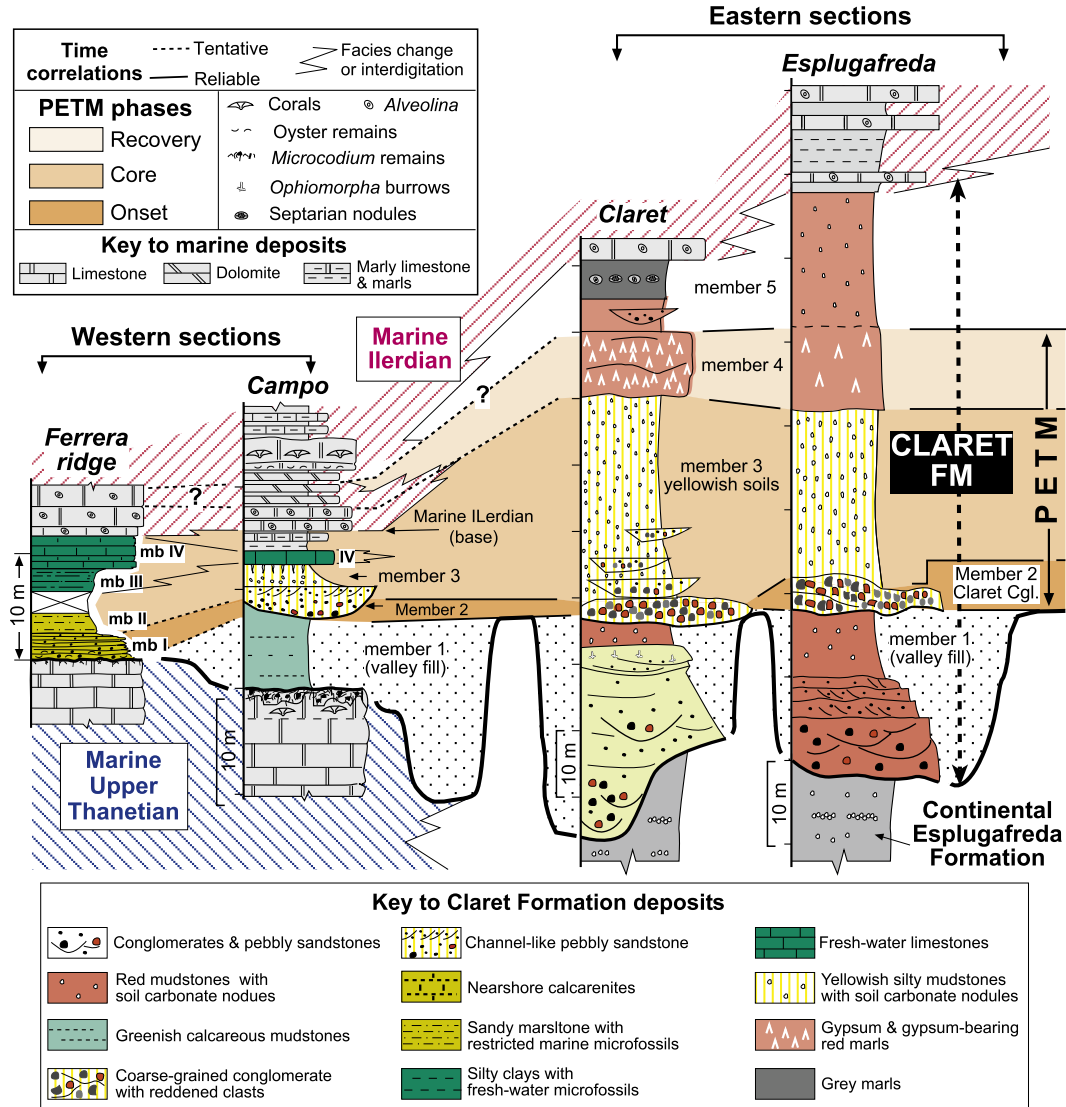


**Fig. 4.** Representative sections across the P-E interval in the Tremp-Graus Basin (location in Fig. 2B), with reliable and tentative correlations of the nine members of the Claret Formation based on  $\delta^{13}\text{C}$  isotopic data from soil carbonate nodules and from organic carbon.

Unit U (15 m) is more relevant for this study and it is therefore described more extensively. It has long been known that this unit is capped by a sharp irregular surface rich in *Microcodium* remains (e.g., Eichenseer and Luterbacher, 1992), a proof of subaerial exposure. Indeed, *Microcodium* is customarily interpreted as the product of the calcification of roots of terrestrial plants on carbonate-rich substrates (Klappe, 1978; Kosir, 2004; but see also Kabanov et al., 2008). However no detailed analysis of this surface has previously been attempted.

The observations presented here were facilitated by two circumstances, the enlargement of the road, which created a fresh cut in unit U, and a landslide triggered by heavy rains in the winter of 2010 providing a wide plain-view exposure of its capping surface (Supplementary Fig. 7A). Three successive intervals could thus be recognised in the uppermost metres of unit U, labelled X, Y and Z in Fig. 9 and in Supplementary Fig. 7A.

Intervals X and Y, despite different grey colouring, are both represented by massive coralgal bindstones. In this study occasional *Microcodium* rosettes were observed in thin sections from the upper part of interval Y (Fig. 9).

Interval Z (1–1.5 m thick), which Scheibner et al. (2007) described as a mixture of coralgal bound-rudstone and macroid boundstone microfacies types, has a brecciated appearance, being formed by dark-

grey irregular zones surrounded by a light-grey or brownish pseudomatrix (Fig. 9B, D, E). Polished slabs and thin sections reveal that the pseudomatrix is mostly composed of *Microcodium* remains, mainly disaggregated prisms with occasional rosettes, while the dark-grey zones, which range in size from 1 cm to a few dm, are irregularly-shaped pieces of host-rock similar in composition to those of intervals X and Y. The thin-sections further prove that the irregular shapes of the host rock pieces are due to corrosion by *Microcodium*. Yet no individual rhizoliths (in the sense of Klappe, 1980) have been recognised, a fact attributed to extensive reworking by the roots of colonising plants. The top surface of interval Z has an undulating morphology with a relief of ca. 50 cm, probably resulting from karstic dissolution during subaerial exposure (Fig. 9A), and it has a centimetric micro-relief due to differential erosion of the more resistant host rock remains and the less resistant *Microcodium*-rich pseudomatrix (Fig. 9C). The features of interval Z, and of its capping surface, are thus clearly attributable to a long-lasting period of subaerial exposure.

A cross-section constructed after the careful mapping of the Campo sector demonstrates that the exposure surface described above is situated in the shoulder of an erosional depression excavated into the uppermost Thanetian carbonates, which is ca. 5 km wide and about 15 m deep in its central part, where unit U was entirely eliminated

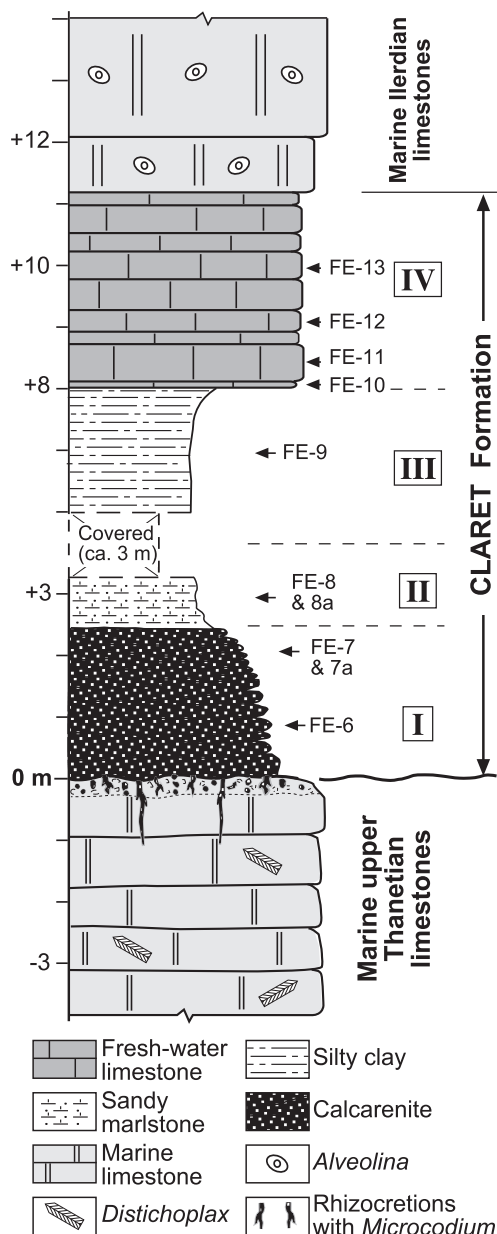


**Fig. 5.** Columnar section across the P-E interval at the Ferrera ridge (location in Fig. 2B), with indication of members I–IV and situation of the samples used for organic carbon isotope analysis (results in Table 1).

(Fig. 8B, C). Member 1 deposits infilling this erosional depression, which range in thickness from ca. 7 m at the Campo section to ca. 23 m at the deepest part of the depression (Fig. 8C), are mostly composed of greenish, weakly calcareous mudstones with a few intercalated calcarenites. Except for occasional inner moulds of gastropods the mudstones are devoid of macrofossils, (Pujalte et al., 2009b). However, charophyte oogonia were found in sample CP-5 and ostracods and small benthic foraminifera in sample CP-6 (Table 2). The mudstones are thus attributable to a low-energy brackish-water setting with fresh-water input.

#### 5.4. Ferrera ridge section

The Danian–Ilerdian succession at the Ferrera section is almost wholly made up of shallow marine carbonates, the exception being a ca. 10 m thick mixed clastic-carbonate unit sandwiched between upper Thanhian and lower Ilerdian carbonates. This unit clearly

represents the Claret Formation distal part, as demonstrated by its stratigraphic position and by carbon isotopic data (Table 1, Fig. 4).

The ca. 90 m thick upper Thanhian marine succession at Ferrera is mostly made up of sandy calcarenites rich in nummulitids and, as in Campo, is capped by a sharp surface with *Microcodium* remains. However, the Ferrera surface differs from the one at Campo in several significant features.

First, *Microcodium* is much less abundant at Ferrera and it is mainly concentrated in the uppermost 30 cm of the Thanhian carbonate succession, although minor amounts of it have been observed in samples from 1 m below the capping surface (Fig. 5, Supplementary Fig. 8A). Second, instead of forming a widespread pseudomatrix, *Microcodium* remains at Ferrera tend to be clustered around irregular, sub-vertical cylindrical tubules, which are abundant and up to 1 cm wide in the uppermost 30 cm of the succession but sporadic and just 1–2 mm wide at depth. Due to that clustering most tubules appear surrounded by haloes of a somewhat dark shade, best seen in polished slabs from the uppermost 30 cm (Fig. 5, Supplementary Fig. 8B, C2). The haloes are therefore interpreted as pedogenetic accumulations around roots, and the tubules as rhizocretions (in the sense of Klappa, 1980). The rhizocretions underwent little deformation during burial compaction and may be partly or totally infilled with calcarenites with oyster fragments and small benthic foraminifera of overlying member I of the Claret Formation (Supplementary Fig. 8C). These features demonstrate that the topmost part of the Thanhian carbonates was subaerially exposed, colonised by plants and probably indurated. The colonising plants died and decayed when the area was reflooded by a shallow sea, and some rhizocretions became open voids that were infilled with marine sediments. Clearly, at Ferrera the extent of plant colonisation was less extensive, and the interval of subaerial exposure shorter, than at Campo. This suggests that the pre-PETM lowstand shoreline was placed a short distance to the west of the Ferrera ridge section.

The calcarenites overlying the subaerial exposure surface at Ferrera were deposited during the PETM according to the isotope data (Table 1), coeval deposits to member 1 being therefore absent. Such absence implies either that no erosional depression was excavated in this distal zone or that the Ferrera site was located at the shoulder of an erosional depression.

#### 6. Basal unconformity and member 1 of the Claret Formation: interpretation

The erosional depressions delineated by the lower boundary of the Claret Formation in the Esplugafreda, Claret and Campo sectors are here interpreted as incised valleys using some of the criteria of Boyd et al. (2006); Table 3. It is widely acknowledged that the excavation of incised valleys in the margins of marine basins is mostly triggered by a relative sea-level fall (e.g., Strong and Paola, 2008), the surfaces of subaerial exposure capping marine deposits at the Campo and Ferrera sections providing evidence that this was the case in the Tremp–Graus Basin.

The excavation of an incised valley continues until the sea reaches its lowest level, the valley being filled with sediments during the subsequent sea-level rise. In this process the seaward part of the incised valley may be transformed into an estuary, but fluvial conditions may continue in its landward part (Boyd et al., 2006). This model may explain the lithological differences in member 1 of the Claret Formation, the brackish-water deposits found in the Campo sector being attributable to an estuarine setting, the red clastic deposits of the Esplugafreda sector to a fluvial setting, those of the Claret sector showing mixed influences.

Field data demonstrate that the cutting and filling of the Tremp–Graus incised valleys occurred during a single cycle of sea-level change prior to the deposition of the Claret Conglomerate (Figs. 6–8), and hence before the onset of the PETM.

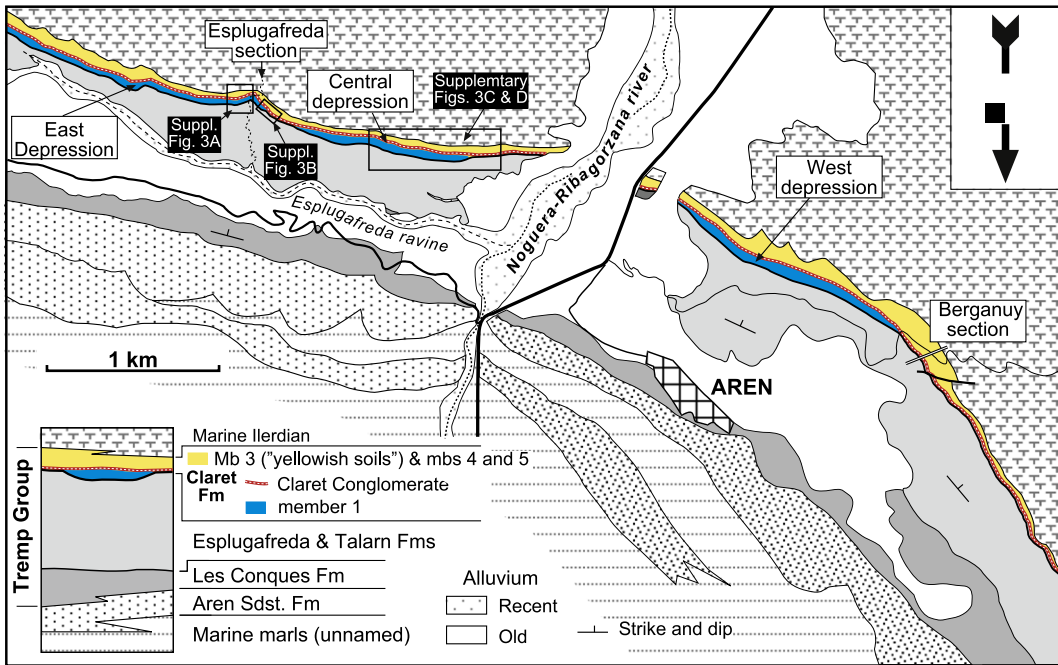


**Fig. 6.** Geological map of the Esplugafreda sector (location in Fig. 2B), showing the five members of the Claret Formation and the three erosional depressions (interpreted as incised valleys) recognized in the area. North is to the bottom of the figure.

## 7. PETM members of the Claret Formation

### 7.1. Member 2 (Claret Conglomerate)

The facies of the Claret Conglomerate change progressively across the Tremp-Graus Basin. In the north-eastern part of the basin it is represented by a sheet-like unit of clast-supported calcareous conglomerates and pebbly calcarenites that can be traced in strike and dip sections from Esplugafreda to the west of Serraduy (ca. 25 km), and from Esplugafreda to near the village of Tendrui, north of Claret (ca. 8 km) (Schmitz and Pujalte, 2007; Figs. 2, 3, 6; Supplementary Figs. 2, 3). This extensive sheet-like unit generally ranges in thickness between 1 and 4 m, locally reaching 8 m, and it is very coarse-grained, some of its well-rounded clasts reaching 80 cm in length, and clasts in the 20–40 cm range being common. A distinctive feature of the unit is the abundance of rubefied (reddened) clasts, which in some exposures amount to almost half the total clast population. Soil carbonate nodules included in intercalated grey or red mudstones in some sections (e.g., Berganuy, Supplementary Fig. 1) provide  $\delta^{13}\text{C}$  isotopic values characteristic of the onset of the PETM (Schmitz and Pujalte, 2007). The sheet-like part of the Claret Conglomerate has a low-relief sharp base and an abrupt top that usually preserves depositional morphologies, a fact attributed to abandonment of depositional tracts after avulsions (Supplementary Figs. 3, 4, 9).

Schmitz and Pujalte (2007) interpreted this part of the Claret Conglomerate as an extensive braidplain, representing the proximal part of a megafan developed at the onset of the PETM after a dramatic increase in seasonal rain. A tectonic origin was excluded by the lack of evidence of regional tectonism (Fig. 1) and by the abrupt lower and upper boundaries of the unit, for it seems unrealistic that tectonism could create and destroy a high relief in the short time span represented by the Claret Conglomerate. Conversely it has been shown through modelling that an increase in catchment precipitation results in the deposition of a laterally extensive sheet of coarse gravel (Armitage et al., 2011).

The Claret Conglomerate is missing near Tendrui but it reappears, about 1 km south of that village, in the Claret sector (Fig. 7). There,

the Claret Conglomerate can be traced for about 2 km and exhibits a lens-shaped geometry, with a nearly flat erosional base and a convex-up top (Fig. 7). Such lens-shaped geometry, also observed a few km west of Serraduy, is thought to reflect a depositional lobe of the Claret Conglomerate megafan.

Further west, in the Campo sector (Fig. 2), Member 2 is represented by numerous channel-like bodies, 2–4 m thick and tens of metres wide, embedded within marly clays. The channel-like bodies are made up of conglomerates and/or pebbly sandstones grading up to cross-bedded and parallel-laminated sandstones with mudstone intercalations. Clasts of the conglomerates rarely exceed 5 cm in length but they are of a similar composition to those at Esplugafreda and Claret, in all cases being mainly derived from Cretaceous limestones. Soil carbonate nodules from mudstone intercalations at the top of some channel-like bodies and from their surrounding marly clays produced PETM isotopic values (Schmitz and Pujalte, 2007; Pujalte et al., 2009b), clear evidence that these deposits are the distal correlative of the sheet-like and lens-shaped segments of the Claret Conglomerate.

### 7.2. Member 3 ("yellowish soils")

Member 3 is mainly made up of silty mudstones of a distinctive yellowish orange colour in weathered exposures (Supplementary Figs. 3, 7), with minor intercalations of channel-like bodies of pebbly sandstones. The unit generally decreases in thickness from east to west, from a maximum of ca. 30 m in the Claret sector to a minimum of ca. 2 m in the Campo section, the decrease being partly due to interfingering with other members (Fig. 4). Another characteristic feature of member 3 is the occurrence of abundant, small-sized (<cm) carbonate nodules that are not concentrated on discrete K horizons but randomly dispersed throughout the unit (Fig. 4, Supplementary Fig. 9, inset). Such nodule distribution suggests a cumulative soil profile (in the sense of Wright and Marriot, 1996), a profile that develops where small but frequent increments of sediments produce aggradation of the sediment surface, vertical displacement of the zone of active pedogenesis and abandonment of lower levels of the soil. Isotopic values of these nodules are typical of the core of the PETM (Schmitz and

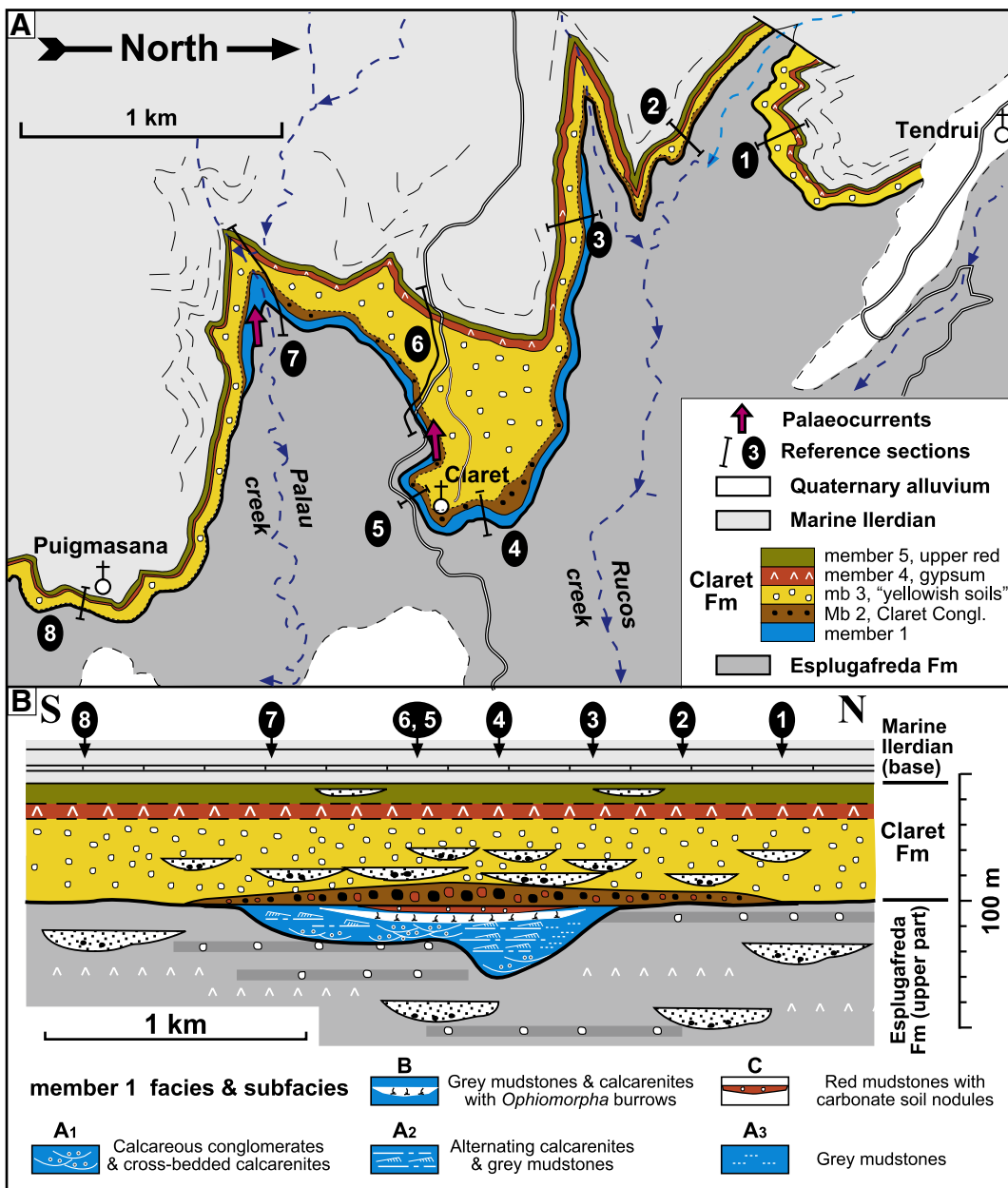


**Fig. 7.** (A) Geological map, and (B) S–N cross-section across the P–E interval in the Claret sector (location in Fig. 2B), showing the position of reference sections and the architecture of the 5 members of the Claret Formation. For lithological key of members 2–5 see Fig. 4.

Pujalte, 2003, 2007; Pujalte et al., 2009b; Supplementary Fig. 1). Rhizoliths are also numerous in some sections (Supplementary Fig. 9, inset).

### 7.3. Members 4 (gypsum-rich member)

Member 4, which is typified by a variable content of gypsum, only occurs in the eastern part of the basin, directly above the yellowish soils (Fig. 4, Supplementary Figs. 1, 9). In the basin margins (i.e. Esplugafreda sector and south of the Claret sector), it is up to 10 m thick and mostly made up of silty mudstones of a deep red colour, the gypsum occurring either as veins, root-like concretions, or centimetre-sized nodules. Instead, gypsum is the predominant lithology of member 4 in the central part of the basin. For instance, in Section 6 of the Claret sector (Fig. 7) the gypsum occurs within two stacked cycles, each 3–4 m thick, composed from bottom to top of three intergradational parts:

1) red siltstone with small gypsum nodules; 2) red siltstone criss-crossed by contorted veins of alabastrine gypsum; and 3) decimetre to metre-sized nodules of massive gypsum, commonly coalescing into larger masses. Finally, in Section 1 of the Claret sector, member 4 is represented by a 4 m thick accumulation almost exclusively made up of alabastrine gypsum (Supplementary Fig. 9).

According to García Veigas (1997), the gypsum of member 4 is of secondary origin after a number of sulphate lithofacies. Nodular-massive gypsum accumulations of the central part of the basin are interpreted as free or subaqueous precipitates within a saline lake, whereas those of the northern and southern parts are considered interstitial precipitates within saline mud-flats surrounding the lake. Clearly an arid climate prevailed in the Tremp-Graus Basin during the recovery phase of the PETM, while member 4 was being deposited.

Interestingly, a carbonate unit also indicative of arid climate was reported by Eichenseer and Luterbacher (1992) at the Campo section, just

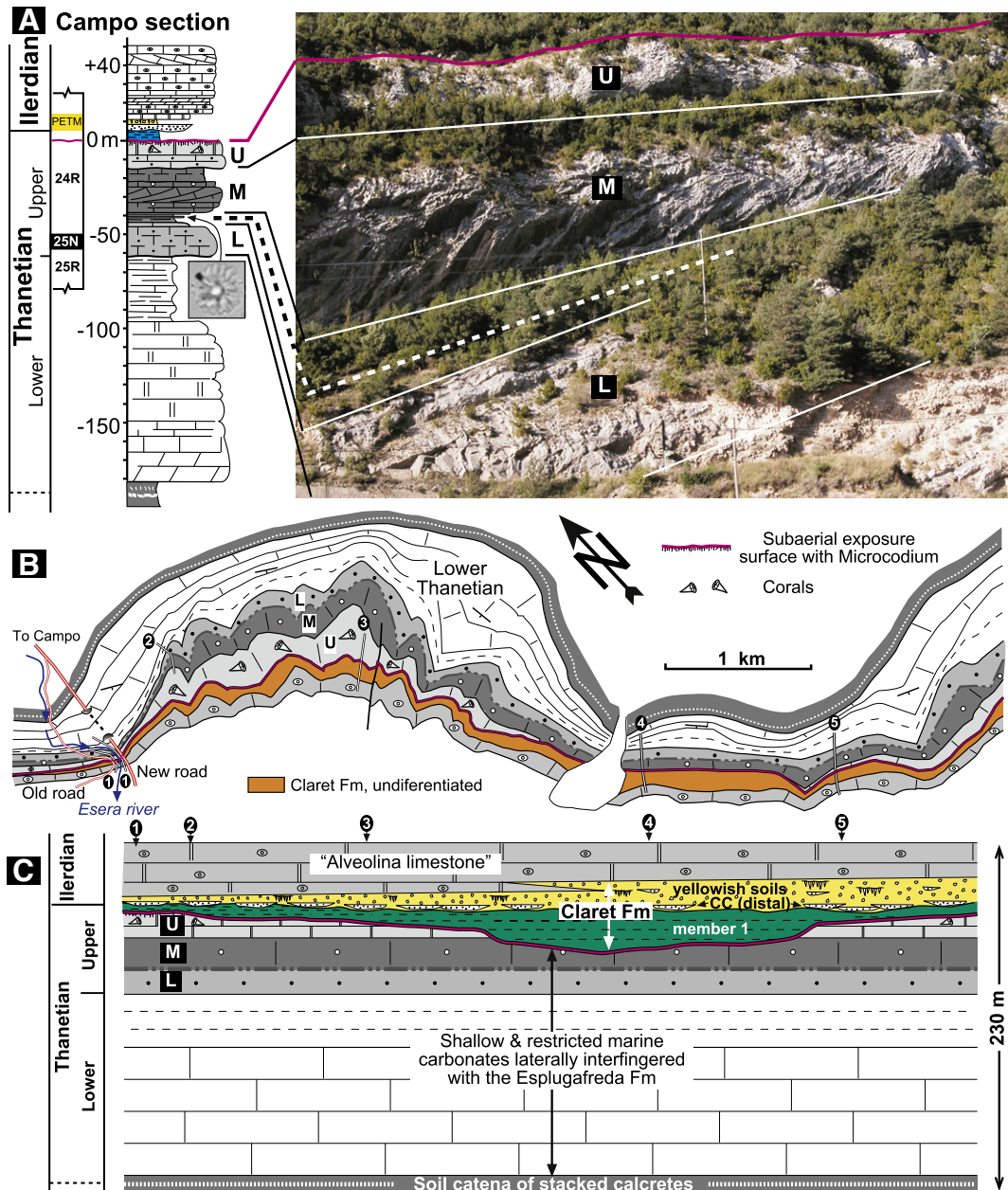


**Fig. 8.** (A) Columnar section and field photo of the Thanetian-lower Ilerdian interval of the Campo section in the right (west) bank of the Esera river. L, M and U = lower, middle and upper units of the Upper Thanetian marine succession; position of geomagnetic chron 25 N, and a micrograph of *Discoaster multiradiatus* is also shown. (B, C) Geological map and cross-section of Thanetian-lower Ilerdian strata in the Campo sector (location in Fig. 2B), highlighting the members of the Claret Formation (CC = Claret Conglomerate distal facies). Reference Sections: 1, Campo; 2, La Cinglera; 3, San Martín; 4, Castellar; 5, Unnamed.

above two prominent limestone beds with alveolinids that pinch out into the yellowish soils about 3 km to the east of Campo (Pujalte et al., 2009b; Fig. 4, Supplementary Fig. 7B). That carbonate unit is ca. 5 m thick and consists of a few stacked shallowing-up cycles composed, from base to top, of lagoonal miliolid packstones, inter- to supratidal limestones with charophytes and supratidal dolomites with algal laminations disrupted by nodules of gypsum and celestine (Supplementary Fig. 8C). Eichenseer and Luterbacher (1992) interpreted these cycles as arid to semi-arid tidal flat parasequences, and pointed out that similar accumulations are absent in the remainder of the marine Ilerdian succession of the Tremp-Graus Basin. The uniqueness of these arid tidal flat deposits, and their stratigraphic location just above deposits coeval with the yellowish soils, strongly suggest that they are correlative with member 4 of the Claret Formation (Fig. 4).

#### 7.4. Claret Formation members at the Ferrera ridge section

Member I (2.5 m thick) is represented by cross- and parallel-laminated calcarenites that decrease up section in bed thickness from 30 cm to 10 cm, and in mean grain-size from medium to very-fine grades (Fig. 5; Supplementary Fig. 8). The calcarenites are well sorted and contain ca. 15% of quartz grains. Abraded oyster remains occur in the lower half of the member, and small benthic foraminifers and calcareous algae in the upper half. Member I is thus attributable to a high-energy nearshore marine environment.

Member II (ca. 2 m thick), which is partly covered by scree and vegetation (Fig. 5; Supplementary Fig. 8), is made up of brownish sandy marlstones grading up into marls. A sample from its lower part (SF-8 in Table 2) contains ostracods and small benthic foraminifera, with

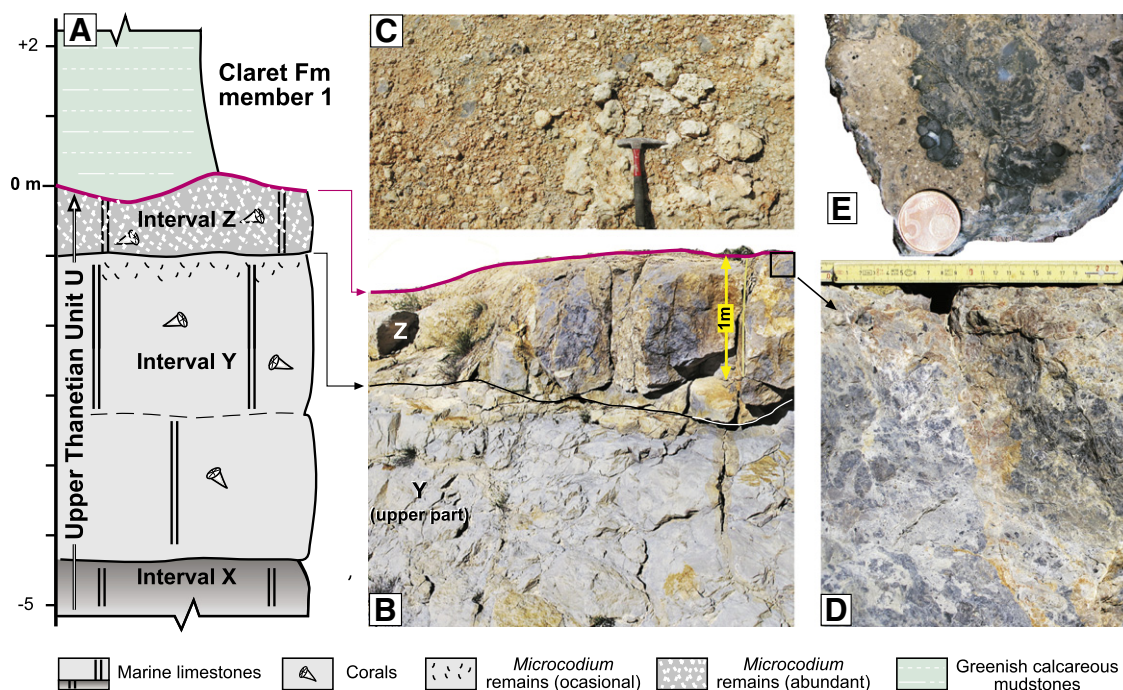


**Fig. 9.** (A) Simplified columnar section of a part of the Campo section in the left (east) bank of the Esera River (location in Fig. 8B). (B) Field view of intervals Y and Z, illustrating their different aspect; note the undulating morphology of the subaerial exposure surface capping Z. (C) Close-up of the rugged surface of subaerial exposure capping interval Z; (D and E) close-up and polished slab of interval Z, showing irregular pieces of host rock (dark grey zones) surrounded by *Microcodium*-rich zones (light-grey zones). Rule in D is 20 cm, diameter of coin in E is 2 cm. Brownish colours in figures B, C and D is due to superficial coating.

lesser amounts of charophyte oogonia and inner moulds of tiny gastropods. The ostracod assemblage is dominated by *Neocyprideis*, a genus reported from Cenozoic shallow marine environments (e.g., Siddiqui, 2000). The benthic foraminifera assemblage is mainly composed of hyaline forms of the order Rotaliida, suborder Rotaliina, a group of foraminifera usually found in shallow marine mixed muddy-sandy floors. The assemblage includes a few quinqueloculiniforms miliolids and rare agglutinated foraminifera, which support the above interpretation. The rare oogonia in sample SF-8 are rather abraded and were probably resedimented.

Member III (ca. 3 m thick; Fig. 5), also poorly exposed (Fig. 5), is exclusively composed of greenish silty clays that only contain a sparse microfossil assemblage of charophytes, mostly stem remains and rare oogonia (sample SF-9 in Table 2). Charophyte stems, unlike oogonia, are too fragile to survive long-distance transport, and are therefore considered to be autochthonous or para-autochthonous. Their occurrence,

coupled with the fine-grained nature of the deposits, point to a freshwater low-energy aquatic environment.

Member IV (3.15 m thick; Fig. 5) is composed of fine-grained limestones, dark-grey in fresh cut, which contain charophyte remains and thin-shelled non-ornamented ostracods, both indicative of a low-energy lacustrine setting. Member IV is also represented in the Campo section by a 1.3 m thick bed of grey micritic limestone (Fig. 4, Supplementary Fig. 7B). Occasional fragments of charophyte stems were observed in thin sections, but also poorly developed circumgranular cracks, mottling and etched quart grains, features indicative of palustrine conditions (e.g., Alonso-Zarza, 2003) that suggest that member IV at Campo was deposited in a zone with an oscillating water-table or seasonally inundated, probably the margin of a fresh water pond or lake. This interpretation is supported by the fact that the limestone bed pinches out within the continental yellowish soils just a few hundred metres to the east of Campo (Pujalte et al., 2009b).

**Table 3**

Comparing some of the criteria for Incised valley systems of Boyd et al. (2006) and observed features of the basal erosional boundary and member 1 of the Claret Formation.

Criteria of Boyd et al. (2006)	Observed features
1 (p. 192) – The valley is a negative (i.e., erosional) palaeotopographic feature, the base of which truncates underlying strata. The valley should be larger than a single channel and commonly has an erosional relief of 10 m or more. Most valleys range in width between 1–10 km.	The depressions in the Esplugafreda, Claret and Campo section are bounded below by erosional surfaces that truncate underlying strata. They range between 15–30 m in erosional relief and between 1.05–5 km in width.
2 (pp. 192 and 193) – The (erosional) base and walls of the valley ... correlates to an erosional (or hiatus) surface outside the valley...that may be characterized by a well-developed soil or rooted horizon.	The surfaces of subaerial exposure with <i>Microcodium</i> in the Campo and Ferrera sections clearly correlate with the erosional bases of the paleovalleys.
4 (p. 194) – Where the area lies close to the shoreline coastal regression accompanies incision (and) the base of the incised-valley fill exhibit a juxtaposition of more proximal (landward) facies over more distal (seaward) deposits across a regional unconformity.	The subaerial exposure surfaces with <i>Microcodium</i> separates Thanetian marine carbonates from non-marine deposits of member 1 at the Campo section, and Thanetian open marine carbonates from littoral-marine deposits of member 1 at the Ferrera section.
5 (pp. 193 and 194) – Deposits of the incised-valley fill onlap the valley base and walls.	Onlap onto the valley wall can be observed in some outcrops (e.g., Supplementary Fig. 3B) and it is inferred for several others (e.g., Fig. 7).
7 (p. 194) Channels contained within the valley should be substantially smaller than the valley itself.	Channels contained within the Esplugafreda and Claret depressions meet that requirement (e.g., Supplementary Fig. 3D).

Isotope data (Table 1) demonstrate that the four members of the Claret Formation at Ferrera belong to the PETM. Member I, because of its coarse-grained nature, is tentatively correlated with the Claret Conglomerate, while overlying members II, III and IV are considered correlative of the yellowish soils, an inference supported by their field relationships (Fig. 4).

## 8. Borehole data

A better delineation of the palaeogeographical evolution of the Tremp-Graus Basin across the P-E interval can be attained with information from four oil exploration wells (location in Fig. 2). In short, the succession of the Cajigar borehole is similar to that of the Serraduy section, those of the Centenera-2 and Monesma wells are comparable to that of the Campo section, and the P-E interval of the Graus-1

borehole is similar to that of the Ferrera ridge section (Supplementary Fig. 10).

## 9. Sea-level changes in the Tremp-Graus Basin across the P-E interval

### 9.1. Reconstruction

A reconstruction of relative sea-level changes in the Tremp-Graus Basin during the P-E interval is graphically illustrated in Fig. 10. Clearly, a transgression took place during late Thanetian times, at the peak of which the sea reached the Serraduy section (1 in Fig. 10). A period of sea-level lowering ensued, during which the former marine carbonate platform became subaerially exposed, first at Campo and then at the Ferrera ridge (2 and 3 in Fig. 10). Concurrently, incised valleys were progressively excavated in the coastal alluvial plain and in the adjacent

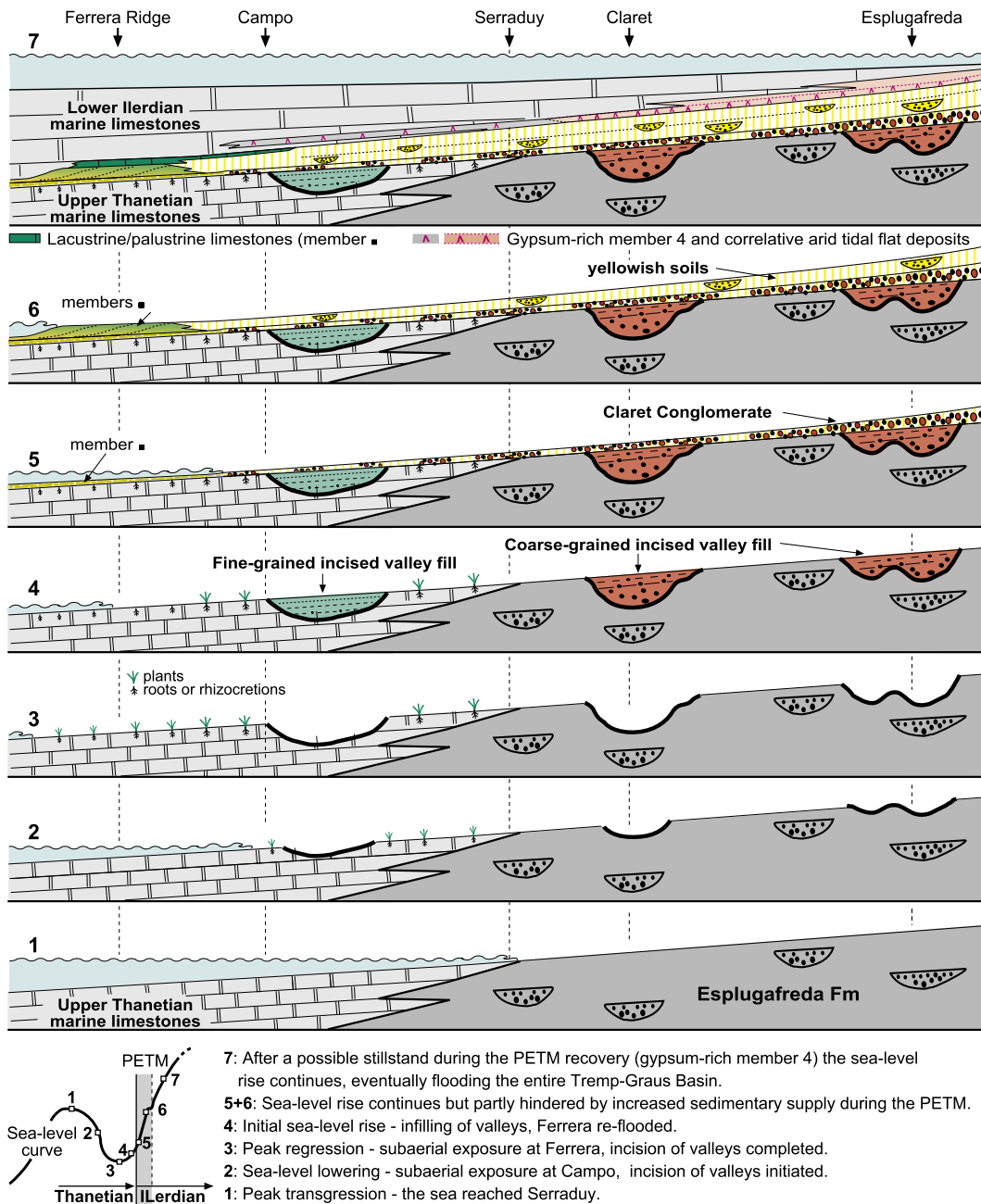


**Fig. 10.** Cross-sections depicting successive positions of the sea level across the P-E interval in the Tremp-Graus Basin. Explanation within the text.

carbonate platform until the sea level reached its lowest point (3 in Fig. 10). The valleys are drawn without deposits for simplicity, although in all probability they contained a fraction of them.

A long period of sea-level rise was then initiated, the infilling of the incised valleys being its first consequence (4 in Fig. 10). This inference is partly based on the fact that most incised valleys are infilled during relative sea-level rises (e.g., Boyd et al., 2006; Strong and Paola, 2008), but it is also supported by the estuarine deposits of member 1 in the Campo sector and the occurrence of *Ophiomorpha* burrows at Claret, both facts indicative of marine influence.

The sea level continued rising during the PETM interval, as demonstrated by the re-flooding of the Ferrera section recorded by member I (5 in Fig. 10). There is ample evidence in the Pyrenean basins that continental clastic influx to the sea was greatly intensified during the PETM interval (e.g., Schmitz et al., 2001; Schmitz and Pujalte, 2003). Based on that, the vertical passage of member I to the muddy shallow marine deposits of member II and then to the fresh-water clayey deposits of member III at the Ferrera section is attributed to a climatically-forced depositional regression (6 in Fig. 10). To the east of Ferrera the sea-level rise caused fluvial aggradation in the coastal plain, recorded by the bulk of the yellowish soils. The lacustrine/palustrine limestones of member IV further reveal that the eastward advance of the Ilerdian sea was heralded by the development of coastal freshwater ponds, probably favoured by a rising water table linked to the sea-level rise (6 and 7 in Fig. 10).

The encroachment of arid tidal flat conditions over marine deposits at Campo suggests a brief pause or slowing down of the sea-level rise during the recovery phase of the PETM (Fig. 10; Supplementary Fig. 7). After this pause the transgression resumed, the Ilerdian sea eventually flooding the entire Tremp-Graus Basin (7 in Fig. 10). It is important to emphasise, however, that the Ilerdian Sea did not reach the Serraduy section, where the late Thanetian highstand shoreline was situated, until the end of the PETM (Fig. 10; Supplementary Fig. 2). This fact entails that the bulk of the PETM took place with a rising but relatively low sea level.

## 9.2. Age models

While it is clear that the sea-level fall and rise causing the excavation and infilling of the Tremp-Graus palaeovalleys pre-date the PETM, the low chronostratigraphic resolution of fossils from the P-E interval preclude their precise timing. Consequently, tentative age models based on two different lines of reasoning are discussed below.

The first model is based on sedimentation rates during Claret Formation times. Estimated time spans for the onset plus the core of the PETM range from 125 to 135 kyr (Giusberti et al., 2007; Röhl et al., 2007; McInerney and Wing, 2011), a mean duration of 130 kyr being therefore used for the model. These 130 kyr are represented in the Tremp-Graus Basin by the Claret Conglomerate plus the yellowish soils, whereas the time interval from the peak lowstand to the onset of the PETM is recorded by member 1 of the Claret Formation (Figs. 4, 10). Two facts, however, must be taken into account before the estimate is attempted. One, member 1 deposits only occur within the incised valleys, while those of the PETM are expansive over the whole eastern area of the basin (Figs. 4, 10). Two, sedimentation rates increased in the Tremp-Graus Basin during the PETM (Schmitz and Pujalte, 2003). To overcome the first issue, the outcrop areas of members 1–3, rather than their local thicknesses, have been taken as a proxy of sedimentation rates. For the second, estimates are made for scenarios involving double, triple and quadruple increases. Larger increases are considered unlikely since, as explained above, sedimentary features of member 1 also indicate comparatively high sedimentation rates.

The outcropping area of Members 2 and 3 in the Esplugafreda and Claret sectors have been calculated to be between 6 and 8 times larger than those of member 1 (7 times on average). If no increase in sedimentation rate during the PETM is taken into account, the time span of

member 1 would be ca. 18.6 kyr (i.e. 130 kyr/7). This figure would successively augment to 37.1, to 55.7 and to 74.3 kyr in the two-fold, three-fold and four-fold increase scenarios. It is reasonable to conclude that the peak lowstand occurred 75 kyr, or less, prior to the PETM.

The second line of approach, based on the deep-water Zumaia section (location in Fig. 2A), provides a similar estimate. At Zumaia the bulk of the upper Thanetian is formed by stacked marl/marly limestone couplets 40–50 cm thick, with intercalated thin-bedded (0.5–3.5 cm) turbidites. This succession, however, is capped by three limestone beds separated by thin marly intercalations, each bed being ca. 20 cm thick, the lower one including a turbidite 8 cm thick (Supplementary Fig. 11). These limestones have a distinctive greenish colouring resulting from a high content in glauconite, and are known to be widespread in the Basque Basin (Baceta et al., 2000; Schmitz et al., 2001). The onset of the PETM occurs immediately above the uppermost limestone bed (Schmitz et al., 1997; Storme et al., 2012).

Dinarès-Turell et al. (2002) convincingly showed that the upper Thanetian marl/marly limestone couplets at Zumaia are the expression of orbital precession cycles, with a mean duration of ca. 19–23 kyr, and it is reasonable to assume that the thin marl/green limestone couplets also record precession cycles. Insoluble residues in the former (mostly clays and silt-sized quartz grains) range between 80 and 45%, abruptly diminishing to 25–20% in the green limestone couplets (Schmitz et al., 1997; Storme et al., 2012). However, the reason for such a sudden and significant reduction in clastic input has not been discussed so far. It is here suggested that it is linked to the initial phase of the pre-PETM sea-level rise and transgression in the Tremp-Graus Basin (from 3 to 4 in Fig. 10), during which a sizable percentage of the clastic supply was being trapped in the incised valleys. This scenario would satisfactorily explain both the reduction in clastic input and the abundance of glauconite in the green limestone, an indication of condensation. If correct, this would imply that the peak lowstand (i.e. just before the deposition of the three green limestone couplets) occurred about 57–69 kyr prior to the onset of the PETM.

## 9.3. The pre-PETM sea-level fall: magnitude and palaeogeographic effects

An attempt to quantify the magnitude of the pre-PETM sea-level fall, based on data from the Campo section and sector, is graphically depicted in Fig. 11A. The corallal limestones in the uppermost Thanetian unit U prove that, just prior to the peak lowstand, Campo was located in the photic zone of a shallow sea. Estimations of the depositional depth of these limestones are however somewhat vague. For instance, Scheibner et al. (2007) concluded that they were deposited below the wave base, while Baceta et al. (2011) pointed out that their fossil assemblage resembles turbid-water corals living in shallow sheltered positions of sub-littoral areas. Therefore it is conservatively assumed here that the corals grew at 3–5 m water depth, their subsequent subaerial exposure implying a 3–5 m sea-level fall. The excavation of the erosional valley to the east of Campo requires 15 additional metres of sea-level fall (Fig. 8A). Accordingly, the magnitude of the pre-PETM sea-level fall in the Tremp-Graus Basin was, at least, 18–20 m. It should be noted that this estimate applies to the last phase of the fall, as the sea-level lowering from the peak highstand to the peak lowstand (from 1 to 3 in Fig. 10) may have been greater.

Although the magnitude of the sea-level fall remains somewhat imprecise, the palaeogeographic changes it brought about can be accurately reconstructed. The highstand and peak lowstand shorelines can be traced extrapolating the data from, respectively, the Serraduy section and the Cajigar borehole, and the Ferrera ridge section and the Graus-1 borehole (Fig. 11B, C). Clearly, the sea-level fall forced a seaward retreat of the shoreline of ca. 20 km. Also, it triggered the excavation of incised valleys, which decreased in width upstream from ca. 5 km in the Campo sector to around 1 km in the central depression of the Esplugafreda sector (Fig. 11C). The E-W Claret erosional depression, in the axial part of the basin, is tentatively considered a trunk incised valley,

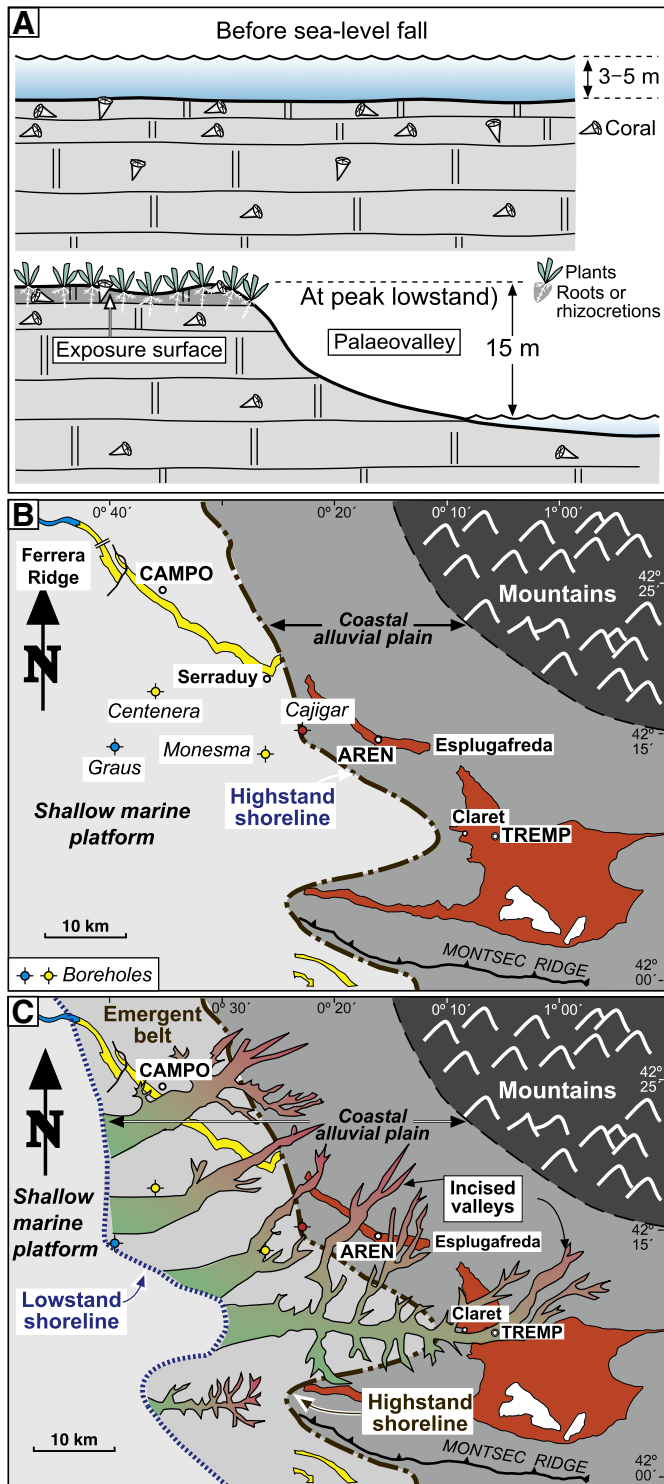


**Fig. 11.** (A) Simplified sketch used to estimate the magnitude of the pre-PETM sea-level fall, based on observations in the Campo section and sector (location in Figs. 2B and 8B). (B and C) Reconstructed palaeogeographies of the Tremp-Graus Basin for the peak transgression and peak regression intervals of the late Thanetian sea (1 and 3 in Fig. 11).

whereas the NNE–SSE trending valleys of the Esplugafreda sector are interpreted as tributaries. The areal distribution of the valleys, coupled with palaeocurrent directions, demonstrate that several incised valley systems must have existed, from which it is concluded that the sea-level fall prompted the excavation of a whole suite of them (Fig. 11C).

## 10. Sea-level changes across the P–E interval in other basins

Sea-level changes similar to those recognized in the Tremp-Graus Basin across the P–E interval have been described elsewhere in the Pyrenees, in the North Sea area, in the Austrian Alps (northern margin of the Tethys), and in the Nile Valley (southern margin of the Tethys).

In the Ordesa and Monte Perdido National Park (north of the Ainsa Basin, south-central Pyrenees; Fig. 1), Robador et al. (2009) and Pujalte et al. (2011) reported that continental pebbly quartz sandstones abruptly overlie an irregular erosional surface carved into upper Thanetian marine carbonates, a facies shift indicative of a sea-level fall. The continental quartz sandstones evolve gradually seaward to nummulite-bearing sandy marls attributable to the PETM, and are overlain by lower Ilerdian marine limestones recording a subsequent sea-level rise and transgression.

South of Bilbao, in the western Pyrenees (Fig. 2A), incised valleys infilled with continental quartz sands were described by Floquet (1992) and by Baceta et al. (1994). No isotopic analyses were carried out in these studies, but the incised valley deposits are sandwiched between upper Thanetian and lower Ilerdian marine carbonates, a stratigraphic position identical to those in the Tremp-Graus Basin. It is reasonable to assume, therefore, that their respective ages are similar.

The occurrence of incised valleys in the North Sea just below the P–E interval area has long been known (e.g., Vandenberghe et al., 1998). In the Cap d'Ailly area (Normandy, France) the P–E interval begins, according to Dupuis (2000), with a unit of fluvio-deltaic sands and sandstones that infills an irregular topography excavated into Upper Cretaceous chalks. These sands are overlain by lacustrine–palustrine limestones and marls with pedogenic features in turn capped by a 1 m thick bed of lignite in which the CIE associated with the PETM was recorded. The succession continues with alternating clays, silts and sands with abundant lagoonal fauna. Dupuis (2000) attributed the incised topography into the chalk to a period of low sea-level, followed by a sea-level rise that successively caused the infilling of the channel-like depressions, aggradation of the coastline and deposition of the lagoonal succession. The occurrence of the CIE in the 1 m thick lignite proves that both the lowstand and the onset of the sea-level rise predate the PETM. Dupuis et al. (2011) subsequently proved that the same situation can be observed in outcrops across the eastern English Channel, northwestern France and southern Belgium.

Sea-level changes in the Austrian Alps were investigated Egger et al. (2009) and Egger (2011) in two sections, Frauengrube and Anthering. The former is a shallow-water succession in which the PETM interval is missing, the latter a deep-water turbidite-bearing succession with a continuous record across the P–E interval. The thickest turbidites at Anthering, some of them up to 5 m thick, occur in the 20 m thick interval situated just below the onset of the PETM. This fact was taken as evidence of a sea-level fall occurring shortly before the PETM, which would also explain the missing interval at Frauengrube. During the PETM interval itself, sedimentation at Anthering was mainly of a fine-grained nature, with a large increase in hemipelagic contribution, features considered indicative of a coeval sea-level rise.

In the Nile Valley, the P–E interval is represented by an outer shelf succession that contains an expanded record of the PETM, the base of which marks the Global Boundary Standard Stratotype Section and Point (GSSP) for the Eocene Series (Aubry et al., 2007). This GSSP was placed at the base of the so-called Dababiya quarry beds, a unit resting on a gently, concave-up erosional surface of regional extent excavated in the uppermost Paleocene succession, the origin of which has been linked to a pre-PETM sea-level fall (Speijer, 2006; Aubry et al., 2009). Based on a quantitative analysis of ostracod associations Speijer and Morsi (2002) concluded that the magnitude of the fall was ca. 15 m, it took place during the 60 kyr prior to the PETM and it was followed by a sea-level rise of ca. 20 m during the PETM, leading to the deposition of the Dababiya Quarry Beds. Thus, although based on an entirely

different data set, the Egyptian record seems to closely match the timing and magnitude of the sea-level changes described in the Tremp-Graus Basin.

## 11. Discussion

Several authors have suggested that sea-level changes across the P-E interval in the North Sea area were tectonically induced. Dupuis et al. (2011), for instance, concluded that the incision of the pre-PETM fluvial network was a result of a broad uplift caused by magmatic activity in the North Atlantic Igneous Province, while the subsequent transgression was caused by thermal subsidence of the margins after the cooling of the intrusion. Tectonomagmatic driven uplift and subsidence might also be invoked to explain the sea-level changes in the Austrian Alps, where the effect of North Atlantic volcanism is well documented (Egger and Brückl, 2006). However, those in the Pyrenees would be difficult to explain by this mechanism for at least two reasons: one, tectonics were subdued in the Pyrenees during the Danian–early Ilerdian interval (Fig. 1); two, dissimilar effects would be expected in different tectonic units and, instead, essentially the same results were found in the Tremp-Graus Basin, in the northern Ainsa Basin and in the southern Basque Cantabrian area (Figs. 1, 2). The similar timing and magnitude of sea-level changes in the Pyrenean basins and in the Nile Valley would be even harder to explain. The bulk of the evidence therefore suggests that the sea-level changes around the P-E in the Tremp-Graus Basin were either eustatic or at least eustatically-dominated.

The origin of the late Thanetian sea-level lowering is somewhat enigmatic. Glacioeustasy is one possibility, as some recent studies indicate that ephemeral small ice sheets could grow in Antarctica even during greenhouse climates (e.g., Miller et al., 2005a), and in fact Speijer (2006) suggested this mechanism to explain the pre-PETM sea-level fall in Egypt. However, a 20 m lowering of global sea level through glacioeustasy alone would require a major cooling and a rapid buildup of ice, of which published oxygen isotopic records show no evidence. Thus, although glacioeustasy might have played a role, this fact argues strongly against it being the sole driving mechanism of the sea-level fall. Clearly more data will be necessary to resolve the issue.

The eustatic nature of the sea-level rise during the PETM is more conclusive since, in addition than in the basins here reported, the rise has been documented in such widely separated sites as the New Jersey Shelf, Arctic Spitsbergen or New Zealand. In these three sites the rise had been attributed to thermal expansion of seawater due to ocean warming during the PETM (Sluijs et al., 2008; Handley et al., 2011; Harding et al., 2011). However, the data from the Tremp-Basin demonstrate that the sea-level rise started before the PETM and continued during and after it, causing the widespread Ilerdian transgression in the whole Pyrenean Gulf (Fig. 10). Clearly other mechanisms, in addition to thermal expansion, must have forced such a significant and long lasting eustatic sea-level rise. The close temporal coincidence between the rise and tectono-magmatic activity in the North Atlantic strongly suggest a causal relationship, but perhaps not in the way advocated by Dupuis et al. (2011). Alternatively, Miller et al. (2005b) indicate that the opening of the Norwegian–Greenland Sea during the late Paleocene to early Eocene interval was coeval with the largest change in ridge length of the past 100 Myr, and they suggest that this reorganisation caused a sea-level rise and increased CO<sub>2</sub> outgassing which contributed to global warming.

## 12. Conclusions

The data provided in this paper demonstrate that the PETM was preceded in the Tremp-Graus Basin by a sea-level fall of ca. 20 m, which forced a seaward displacement of the shoreline of ca. 20 km and the excavation of a whole suite of incised valleys in the adjacent alluvial plain. The subsequent sea-level rise started between 75 and

57 kyr before the P-E boundary, bringing about the infilling of the incised valleys. Despite a depositional regression at the onset of the PETM, caused by increased clastic supply, the sea level continued to rise during and after the thermal event, causing the aggradation of the alluvial plain and the so-called Ilerdian transgression. Literature data indicate that the sea-level lowering preceding the PETM can be recognised in other basins of the Pyrenees, throughout the whole North Sea area, the Austrian Alps and in Egypt, and that the subsequent sea-level rise is globally widespread, strong evidence of an eustatic origin. The precise mechanism(s) causing the pre-PETM sea-level lowering still need to be determined, although a glacioeustatic component cannot be excluded. The subsequent global sea-level rise was most probably connected to a large change in ridge length in the Norwegian-Greenland Sea.

Supplementary data to this article can be found online at <http://dx.doi.org/10.1016/j.palaeo.2013.10.016>.

## Acknowledgements

Field and laboratory studies of VP and JIB were funded by the Research Project CLG2011-23770 (Ministerio de Economía y Competitividad, Spanish Government) and IT-631-13 (Research Groups of the Basque University System, Basque Government); those of BS by the Swedish Research Council. We are indebted to A. Pérez-García (Repsol Exploración SA) for the borehole information, to F. Caballero (University of the Basque Country) for assistance in the field and sample preparation, and to J. Rodriguez-Lázaro and B. Martínez García (University of the Basque Country) for their advice about the Claret Formation ostracods and small benthic forams. Last, but not least, we thank three anonymous reviewers and Finn Surlyk (Journal Editor), for numerous comments that greatly improved an early version of this manuscript.

## References

- Alonso-Zarza, A.M., 2003. Palaeoenvironmental significance of palustrine carbonates and calcretes in the geological record. *Earth Sci. Rev.* 60, 261–298.
- Armitage, J.J., Duller, R.A., Whittaker, A.C., Allen, P.A., 2011. Transformation of tectonic and climatic signals from source to sedimentary archive. *Nat. Geosci.* 4, 231–235.
- Aubry, M.P., Ouda, K., Dupuis, C., Berggren, W.A., Van Couvering, J.A., Members of the Working Group on the Paleocene/Eocene boundary, 2007. *The Global Standard Stratotype-section and Point (GSSP) for the base of the Eocene Series in the Dababiya section (Egypt)*. Episodes 30, 271–286.
- Aubry, M.P., Dupuis, C., Berggren, W.A., Ouda, K., Knox, K., Sabour, A.A., 2009. Sea-level changes bracket the PETM. In: Strong, P., Crouch, E., Hollis, C. (Eds.), *Biotic Events of the Paleogene*, CBEP 2009, Wellington, New Zealand, Conference program and Abstracts, p. 144.
- Baceta, J.I., Pujalte, V., Payros, 1994. Rellenos de valles encajados en el Maastrichtiense superior y Paleógeno inferior de Alava (Plataforma Noribérica, Cuenca Vasca). *Geogaceta* 16, 86–89.
- Baceta, J.I., Pujalte, V., Dinarès-Turell, J., Payros, A., Orue-Etxebarria, X., Bernaola, G., 2000. The Paleocene–Eocene boundary interval in the Zumáia section (Guipúzcoa, Basque Basin): magnetostratigraphy and high-resolution lithostratigraphy. *Rev. Soc. Geol. Esp.* 13, 375–391.
- Baceta, J.I., Pujalte, V., Caballero, F. (Eds.), 2006. *Paleocene and Early Eocene facies and events: a basin–platform–coastal plain transect (South-Central and Western Pyrenees)*. Post Conference Field Trip Guidebook of the Climate and Biota of the Early Paleogene International Meeting 2006, Bilbao, Spain (94 pp.).
- Baceta, J.I., Pujalte, V., Wright, V.P., Schmitz, B., 2011. Carbonate platform models, sea-level changes and extreme climatic events during the Paleocene–early Eocene greenhouse interval: a basin–platform–coastal plain transect across the southern Pyrenean basin. In: Arenas, C., Pomar, L., Colombo, F. (Eds.), *Pre-Meeting Field-trips Guidebook, 28th IAS Meeting*, Zaragoza. Sociedad Geológica de España, Geo-Guias, 7, pp. 101–150.
- Boyd, R., Dalrymple, R.W., Zaitlin, B.A., 2006. *Estuarine and incised-valley facies models*. In: Posamentier, H.W., Walker, R.G. (Eds.), *Facies Models Revisited: SEPM (Society for Sedimentary Geology) Special Publication*, 84, pp. 171–235.
- Crouch, E.M., Heilmann-Clausen, C., Brinkhuis, H., Morgans, H.E.G., Rogers, K.M., Egger, H., Schmitz, B., 2001. Global dinoflagellate event associated with the late Paleocene thermal maximum. *Geology* 29, 315–318.
- Cuevas, J.L., 1992. *Estratigrafía del Garumniense de la Conca de Tremp. Prepirineo de Lérida*. Acta Geol. Hisp. 27, 95–108.
- DeConto, R.M., Galeotti, S., Pagani, M., Tracy, D., Schaefer, K., Zhang, T., Pollard, D., Beerling, D.J., 2012. Past extreme warming events linked to massive carbon release from thawing permafrost. *Nature* 484, 87–92.
- Dickens, G.R., O'Neil, J.R., Rea, D.K., Owen, R.M., 1995. Dissociation of oceanic methane hydrate as a cause of the carbon isotope excursion at the end of the Paleocene. *Paleoceanography* 10, 965–971.

- Dinarès-Turell, J., Baceta, J.I., Pujalte, V., Orue-Etxebarria, X., Bernaola, G., 2002. Magnetostratigraphic and cyclostratigraphic calibration of a prospective Palaeocene / Eocene stratotype at Zumaya (Basque Basin, northern Spain). *Terra Nova* 14, 371–378.
- Domingo, L., López-Martínez, N., Leng, M.J., Grimes, S.T., 2009. The Paleocene–Eocene Thermal Maximum record in the organic matter of the Claret and Tendrui continental sections (South-central Pyrenees, Lleida, Spain). *Earth Planet. Sci. Lett.* 281, 226–237.
- Dupuis, C., 2000. L'intervalle Paléocène–Eocène au Cap d'Ailly (Haute Normandie) et les paléoréalisations à la base des faciès Sparnaciens. *Bull. Inf. Géol. Bassin Paris* 37, 10–14.
- Dupuis, C., Quesnel, F., Iakovleva, A., Storme, J.-Y., Yans, J., Magioncalda, R., 2011. Sea level changes in the Paleocene–Eocene interval in NW France: evidence of two major drops encompassing the PETM. In: Egger, H. (Ed.), Climate and Biota of the Early Paleogene, Conference Program and Abstracts, Salzburg, Austria. Berichte der Geologischen Bundesanstalt, 85, p. 113.
- Egger, H., 2011. The early Paleogene history of the Eastern Alps. In: Egger, H. (Ed.), Climate and Biota of the Early Paleogene, Field-Trip Guidebook, Salzburg, Austria. Berichte der Geologischen Bundesanstalt, 86, pp. 9–16.
- Egger, H., Brückl, E., 2006. Gigantic volcanic eruptions and climatic change in the early Eocene. *Int. J. Earth Sci.* 95, 1065–1070.
- Egger, H., Heilmann-Clausen, C., Schmitz, B., 2009. From shelf to abyss: record of the Paleocene/Eocene boundary in the Eastern Alps (Austria). *Geol. Acta* 7, 215–227.
- Eichenseer, H., 1988. Facies geology of late Maestrichtian to early Eocene coastal and shallow marine sediments, Tremp-Graus Basin, northeastern Spain. *Arbeiten aus dem Institut und Museum für Geologie und Paläontologie der Universität Tübingen*, n.1. (273 pp.). (Ph.D. Thesis).
- Eichenseer, H., Luterbacher, H., 1992. The marine Paleogene of the Tremp region (northeast Spain): depositional sequences, facies history, biostratigraphy and controlling factors. *Facies* 27, 119–152.
- Fernández, O., Muñoz, J.A., Barués, P., Falivene, O., 2012. 3D structure and evolution of an oblique system of relaying folds: the Ainsa basin (Spanish Pyrenees). *J. Geol. Soc.* 169, 545–559.
- Floquet, M., 1992. Outcrop sequence stratigraphy in a ramp setting: the Late Cretaceous–Early Paleogene deposits of the Castilian Ramp (Spain). In: CNRS/IPF (Ed.), Field trip guide book International Symposium on Sequence Stratigraphy of Mesozoic–Cenozoic European Basins: Université de Bourgogne, Dijon (130 pp.).
- García Veigas, J., 1997. First Continental Evaporitic Phase in the South Pyrenean Central Area: Tremp Gypsum (Garumna Facies, Upper Paleocene; Allochthonous Zone). In: Busson, G., Schreiber, B.Ch. (Eds.), Sedimentary Deposition in Rift and Foreland Basins in France and Spain (Paleogene and Lower Neogene). Columbia University Press, pp. 335–342.
- Gile, L.H., Peterson, F.F., Grossman, R.B., 1965. The K horizon – a master soil horizon of carbonate accumulation. *Soil Sci.* 99, 74–82.
- Gingerich, P.D., 2003. Mammalian responses to climate change at the Paleocene–Eocene boundary: Polecat Bench record in the northern Bighorn Basin, Wyoming. In: Wing, S.L., Gingerich, P.D., Schmitz, B., Thomas, E. (Eds.), Causes and Consequences of Globally Warm Climates in the Early Paleogene. GSA Special Paper, 369, pp. 463–478.
- Giusberti, L., Rio, D., Agnini, C., Backman, J., Fornaciari, E., Tateo, F., Oddone, M., 2007. Mode and tempo of the Paleocene–Eocene Thermal Maximum in an expanded section from the Venetian pre-Alps. *Geol. Soc. Am. Bull.* 119, 391–412.
- Handley, L., Crouch, E.M., Pancost, R.D., 2011. A New Zealand record of sea level rise and environmental change during the Paleocene–Eocene Thermal Maximum. *Palaeogeogr. Palaeoclimatol. Palaeoecol.* 305, 185–200.
- Harding, I.C., Charles, A.J., Marshall, J.E.A., Pälike, H., Roberts, A.P., Wilson, P.A., Jarvis, E., Thorne, E., Morris, E., Moremon, R., Pearce, R.B., Akbari, S., 2011. Sea-level and salinity fluctuations during the Paleocene–Eocene thermal maximum in Arctic Spitsbergen. *Earth Planet. Sci. Lett.* 303, 97–107.
- Higgins, J.A., Schrag, D.P., 2006. Beyond methane: towards a theory for the Paleocene–Eocene Thermal Maximum. *Earth Planet. Sci. Lett.* 245, 523–537.
- Kabanov, P., Anadón, P., Krumbein, W.E., 2008. *Microcodium*: an extensive review and a proposed non-rhizogenic biologically induced origin for its formation. *Sediment. Geol.* 205, 79–99.
- Klapa, C.F., 1978. Biolithogenesis of *Microcodium*: elucidation. *Sedimentology* 25, 489–522.
- Klapa, C.F., 1980. Rhizoliths in terrestrial carbonates: classification, recognition, genesis and significance. *Sedimentology* 27, 613–629.
- Kosir, A., 2004. *Microcodium* revisited: root calcification products of terrestrial plants on carbonate-rich substrates. *J. Sediment. Res.* 74, 845–857.
- McInerney, F.A., Wing, S.L., 2011. The Paleocene–Eocene Thermal Maximum: a perturbation of carbon cycle, climate, and biosphere with implications for the future. *Annu. Rev. Earth Planet. Sci.* 39, 489–516.
- Miller, K.G., Komink, M.A., Browning, J.V., Wright, J.D., Mountain, G.S., Katz, M.E., Sugarman, P.J., Cramer, B.S., Christie-Blick, N., Pekar, S.F., 2005a. The phanerozoic record of global sea-level change. *Science* 310, 1293–1298.
- Miller, K.G., Wright, J.D., Browning, J.V., 2005b. Visions of ice sheets in a greenhouse world. In: Paytan, A., De La Rocha, C. (Eds.), Ocean Chemistry Throughout the Phanerozoic. *Marine Geology Special Issue*, 217, pp. 215–231.
- Muñoz, J.A., 1992. Evolution of a continental collision belt: ECORS-Pyrenees crustal balanced cross-section. In: McClay, K.R., Buchanan, P.G. (Eds.), Thrust tectonics. Chapman & Hall, London, pp. 235–246.
- Pujalte, V., Schmitz, B., 2005. Revisión de la estratigrafía del Grupo Tremp (“Garumniense”, Cuenca de Tremp-Graus, Pirineos meridionales). *Geogaceta* 38, 79–82.
- Pujalte, V., Dinarès-Turell, J., Bernaola, G., Baceta, J.I., Payros, A., 2003. A reappraisal of the position of Chron C25n in the Campo section (Huesca province, south-central Pyrenees). *Geogaceta* 34, 155–158.
- Pujalte, V., Baceta, J.I., Schmitz, B., Orue-Etxebarria, X., Payros, A., Bernaola, G., Apellaniz, E., Caballero, F., Serra-Kiel, J., Tosquella, J., 2009a. Redefinition of the Ilerdian Stage (early Eocene). *Geol. Acta* 7, 177–194.
- Pujalte, V., Schmitz, B., Baceta, J.I., Orue-Etxebarria, X., Bernaola, G., Dinarès-Turell, J., Payros, A., Apellaniz, E., Caballero, F., 2009b. Correlation of the Thanetian–Ilerdian turnover of larger foraminifera and the Paleocene–Eocene Thermal Maximum: confirming evidence from the Campo area (Pyrenees, Spain). *Geol. Acta* 7, 161–175.
- Pujalte, V., Robador, A., Payros, A., Samsó, J.M., 2011. Sea level changes across the PETM in the Pyrenees, part 2: evidence from a platform interior setting. In: Egger, H. (Ed.), Climate and Biota of the Early Paleogene, Conference Program and Abstracts, Salzburg, Austria. Berichte der Geologischen Bundesanstalt, 85, p. 132.
- Robador, A., 2008. El Paleoceno e Ilerdense inferior del Pirineo occidental: Estratigrafía y Sedimentología. (Ph.D. Thesis) University of the Basque Country, Spain. Publicaciones del Instituto Geológico y Minero de España, Serie Tesis Doctorales 12 (312 pp.).
- Robador, A., Samsó, J.M., Serra-Kiel, J., Tosquella, J., 1990. Field guide. In: Barnolas, A., Robador, A., Serra-Kiel, J., Caus, E. (Eds.), Introduction to the Early Paleogene of the South Pyrenean Basin. Field-Trip Guidebook 1st Meeting ICP Project 286. Instituto Tecnológico Geominero de España, Madrid, pp. 131–159.
- Robador, A., Pujalte, V., Samsó, J.M., Payros, A., 2009. Registro geológico del máximo térmico del Paleoceno Eoceno en el Parque Nacional de Ordesa y Monte Perdido (Pirineo Central). *Geogaceta* 46, 111–114.
- Roest, W.R., Srivastava, S.P., 1991. Kinematics of the plate boundaries between Eurasia, Iberia, and Africa in the North Atlantic from the Late Cretaceous to the present. *Geology* 19, 613–616.
- Röhl, U., Westerhold, T., Bralower, T.J., Zachos, J.C., 2007. On the duration of the Paleocene–Eocene thermal maximum (PETM). *Geochem. Geophys. Geosyst.* 8, 1–13.
- Scheibner, C., Rasser, M.W., Mutti, M., 2007. The Campo section (Pyrenees, Spain) revisited: implications for changing benthic carbonate assemblages across the Paleocene–Eocene boundary. *Palaeogeogr. Palaeoclimatol. Palaeoecol.* 248, 145–168.
- Schmitz, B., Pujalte, V., 2003. Sea-level, humidity, and land-erosion records across the initial Eocene Thermal Maximum from a continental-marine transect in northern Spain. *Geology* 31, 689–692.
- Schmitz, B., Pujalte, V., 2007. Abrupt increase in seasonal extreme precipitation at the Paleocene–Eocene boundary. *Geology* 35, 215–218.
- Schmitz, B., Asaro, F., Molina, E., Monechi, S., von Salis, K., Speijer, R.P., 1997. High-resolution iridium,  $\delta^{13}\text{C}$ ,  $\delta^{18}\text{O}$ , foraminifera and nannofossil profiles across the latest Paleocene benthic extinction event at Zumaya, Spain. *Palaeogeogr. Palaeoclimatol. Palaeoecol.* 133, 49–68.
- Schmitz, B., Pujalte, V., Núñez-Betelu, K., 2001. Climate and sea-level perturbations during the Initial Eocene Thermal Maximum: evidence from siliciclastic units in the Basque Basin (Ermua, Zumaya and Trabakua Pass), northern Spain. *Palaeogeogr. Palaeoclimatol. Palaeoecol.* 165, 299–320.
- Siddiqui, Q.A., 2000. Some species of the genus *Neocyprideis* in the early Tertiary of Pakistan. *J. Micropalaentol.* 19, 1–7.
- Sluijs, A., Brinkhuis, H., Crouch, E.M., John, C.M., Handley, L., Munsterman, D., Bohaty, S.M., Zachos, J.C., Reichart, G.J., Schouten, S., Pancost, R.D., Sinninghe Damsté, J.S., Welthers, N.L.D., Lotter, A.F., Dickens, G.R., 2008. Eustatic variations during the Paleocene–Eocene greenhouse world. *Paleoceanography* 23, PA4216 (18 pp.).
- Speijer, R.P., 2006. Eustasy in the hothouse of the PETM. In: Caballero, F., Apellaniz, E., Baceta, J.I., Bernaola, G., Orue-Etxebarria, X., Payros, A., Pujalte, V. (Eds.), Climate and Biota of the Early Paleogene, CBEP 2006, Bilbao, Spain. Volume of Abstracts, p. 168.
- Speijer, R.P., Morsi, A.M.M., 2002. Ostracode turnover and sea-level changes associated with the Paleocene–Eocene Thermal Maximum. *Geology* 30, 23–26.
- Storme, J.-Y., Devleeschouwer, X., Schnyder, J., Cambier, G., Baceta, J.I., Pujalte, V., Di Matteo, A., Iacumin, P., Yans, J., 2012. The Paleocene/Eocene boundary section at Zumaya (Basque–Cantabrian Basin) revisited: new insights from high-resolution magnetic susceptibility and carbon isotope chemostratigraphy on organic matter ( $\delta^{13}\text{C}_{\text{org}}$ ). *Terra Nova* 24, 310–317.
- Strong, N., Paola, C., 2008. Valleys that never were: time surfaces versus stratigraphic surfaces. *J. Sediment. Res.* 78, 579–593.
- Svensen, H., Planke, S., Malthe-Sørensen, A., Jamtveit, B., Myklebust, R., Eidem, T.R., Rey, S.S., 2004. Release of methane from a volcanic basin as a mechanism for initial Eocene global warming. *Nature* 429, 542–545.
- Thomas, E., 1998. Biogeography of the late Paleocene benthic foraminiferal extinction. In: Aubry, M.-P., Lucas, S., Berggren, W.A. (Eds.), Late Paleocene–Early Eocene Climatic and Biotic Events in the Marine and Terrestrial Records. Columbia University Press, New York, pp. 214–235.
- Vandenbergh, N., Laga, P., Steurbaut, E., Hardenbol, J., Vail, P.R., 1998. Tertiary Sequence Stratigraphy at the southern border of the North Sea Basin in Belgium. In: de Graciansky, P.C., Hardenbol, J., Jacquin, T., Vail, P.R. (Eds.), Mesozoic and Cenozoic Sequence Stratigraphy of European basins, 60. SEPM Special Publication, pp. 119–154.
- Vandenbergh, N., Hilgen, F.J., Speijer, R.P., 2012. The Paleogene Period. In: Gradstein, F.M., Ogg, J.G., Schmitz, M., Ogg, G. (Eds.), The Geological Time Scale 2012. Elsevier, pp. 855–921.
- Wright, V.P., Marriott, S.B., 1996. A quantitative approach to soil occurrence in alluvial deposits and its application to the Old Red Sandstone of Britain. *J. Geol. Soc. Lond.* 153, 907–913.
- Zachos, J.C., Wara, M.W., Bohaty, S., Delaney, M.L., Petrizzi, M.R., Brill, A., Bralower, T.J., Premoli-Silva, I., 2003. A transient rise in tropical sea surface temperature during the Paleocene–Eocene Thermal Maximum. *Science* 302, 1551–1554.